JAERI-M
89-056

OPERATIONAL LIMITS AND DISRUPTIONS IN TOKAMAKS
— STATUS AND APPLICATION TO ITER —

May 1989

Toshihide TSUNEMATSU, J. HOGAN*, K. BORRASS**
F. ENGELMANN** and ITER Physics Group

日 本 原 子 力 研 究 所
Japan Atomic Energy Research Institute

JAERI-Mレポートは，日本原子力研究所が不定期に公刊している研究報告書です。
入手の問合わせは，日本原子力研究所技術情報部情報資料課（〒319-11 茨城県那珂郡東海村）あて，お申しこしください。なお，このほかに財団法人原子力弘済会資料センター（〒319-11 茨城県那珂郡東海村日本原子力研究所内）で複写による実費領布をおこなっております。

JAERI-M reports are issued irregularly.
Inquiries about availability of the reports should be addressed to Information Division Department of Technical Information, Japan Atomic Energy Research Institute, Tokaimura, Naka-gun, Ibaraki-ken 319-11, Japan.

編集兼発行　日本原子力研究所
印　　刷　日青工業株式会社

JAERI-M 89-056

Operational Limits and Disruptions in Tokamaks
- Status and Application to ITER -

Toshihide TSUNEMATSU, J. HOGAN*, K. BORRASS**
F. ENGELMANN** and ITER Physics Group

Department of Thermonuclear Fusion Research
Naka Fusion Research Establishment
Japan Atomic Energy Research Institute
Naka-machi, Naka-gun, Ibaraki-ken

(Received April 18, 1989)

This report contains a concise description on status of knowledge in the area of operational limits and disruption characteristics, based on the results of workshops held during the ITER Definition Phase (1988).

Keywords: ITER, Beta Limit, MHD, Density Limit, Disruption

---

* Oak Ridge National Laboratory, USA

** The Net Team (Max-Planck-Institut fuer Plasmaphysik, Garching, FRG)

JAERI－M　89－056

トカマクの運転限界とディスラプション
－現状とＩＴＥＲへの適用－

日本原子力研究所那珂研究所核融合研究部
常松　俊秀・J. HOGAN*・K. BORRASS**
F. ENGELMANN**・ＩＴＥＲ物理グループ

（1989年4月18日受理）

本報告書は，ＩＴＥＲ共同作業定義段階において検討されたトカマクのベータ値限界，密度限界，ディスラプションに関するデータ評価の詳細をまとめたもので，同時にこれらのデータに基づいた設計へのガイドラインについても記述している。

東海研究所：〒319-11　茨城県那珂郡東海村白方字白根２－４
＊　オークリッジ国立研究所
＊＊　ＮＥＴチーム（マックスプランク・プラズマ物理研究所）

Contents

目　　次

Introduction

This report contains a concise description of the status of knowledge in the area of operational limits and disruptions in tokamaks, based on the results of workshop held during the ITER Definition Phase (1988) and additional information obtained from research workers in tokamak physics; moreover it documents the impact of operational limits and disruptions on ITER as well as the rationals for the guidelines adopted for ITER and the R and D needs in this field.

This report is a collection of three independent parts;
Part I: MHD limits, Part II: Density limit, and Part III: Disruptions.

In Part I, MHD beta limits are assessed from experimental data and theoretical predictions. The effect of alpha particles is also discussed. In Part II, phenomenological scaling of density limit is summarized and semi-empirical scaling of heating power is assessed. Finally, in Part III, disruption characteristics are summarized based on experiments and tentative specification for ITER is presented. In each part, recommendations to ITER physics guideline are derived from present data base.

I . MHD LIMITS

I.1 Importance for ITER

If ITER can be operated stably at high beta its confinement capability is significantly enhanced. One of the approaches for finding possible high beta conditions is to search for the maximum stable beta or g-value ($g=\beta/(I_p/aB_t)$) by optimizing the profiles of plasma pressure and safety factor (or current density), and by optimizing the shape (elongation and triangularity) of the plasma cross section. For systems analysis, it is important to know the ranges of the safety factor and of the elongation where the g-value approaches its maximum value, as well as the dependence of the g-value on the safety factor and the shape of the cross section.

For a given cross section shape, operation in the region $2<q_\psi<3$ is a potentially attractive way to increase the energy confinement time through the increase in the plasma current. Many ideal MHD analyses indicate that for $q_\psi<3$ the stability is sensitive to the current profile near the plasma edge. (In a divertor configuration, q_ψ can be taken to be the safety factor at the 95% flux surface.) A strong degradation of the beta limit appears for $q_\psi<3$ due to external kink modes when the conducting wall is placed at infinity. This degradation is present even for high q values (near large integer q_ψ) when the current density or its derivative at the edge exceeds a certain value. If wall stabilization is essential in this case, it is necessary to assess experimental and computational data on the role of the wall to avoid locked external kink modes during long burning pulses.

The pressure and safety factor (current) profiles needed to achieve stable high beta states may have an important impact on the ignition conditions. The compatibility of the optimized high beta profiles with profiles characteristic of central heating by neutral beams, RF waves and alpha-particles must be considered. Furthermore, the effect of fast ions and alpha-particles on the stability of m=1 modes and the energy and particle confinement in the central region of a plasma column is important.

As mentioned above, higher q (q_ψ>3) is favorable for reaching high beta. One possible way of increasing the energy confinement time, therefore, is to increase κ along with the plasma current without reducing q. At high elongation, there is the possibility that an intrinsic bifurcation of the poloidal magnetic field structure in the MHD equilibrium may appear. Even if this does not appear up to κ~2.5, the problem of passive and active control of the plasma position is very demanding for highly elongated configurations.

The ideal MHD stability is affected by high energy ions. In experiments with neutral beam heating perpendicular to the magnetic filed line, fishbone instability is observed. This may occur when a plasma is heated by alpha particles and may limit the electron temperature at the plasma center. The evaluation of the beta limit by alpha particle induced instability is an important issue for ITER. The effect of alpha particle on ballooning mode is also important to evaluate the pressure gradient near the plasma center as well as the global beta limit.

I.2 Data base on MHD limits

I.2.1 Experimental results on beta and q-limits

(1) DIII-D [1]

In DIII-D, beta and q-limits were investigated for H-mode discharges heated by neutral beams in a divertor configuration. The elongation and triangularity of the cross section were varied in the range $1.2 \leq \kappa \leq 2.2$ and $0 \leq \delta \leq 0.8$, respectively. However, most of the high beta discharges were obtained for $1.6 \leq \kappa \leq 2.0$ and $0.2 \leq \delta \leq 0.4$. The DIII-D tokamak is operated in a single-null point divertor configuration and the triangularity for their data is defined by the average, $(\delta_{upper}+\delta_{lower})/2$. The triangularity increases with elongation because of the coil current programming used for DIII-D operation. Low-q discharges were studied in the same κ range, and the bulk of the data for low q lies also in the range $1.6 < \kappa < 2$. Here, κ, δ and q_ψ are defined at the 95% poloidal flux surface.

The operational limit in a β-I_N diagram is shown in Fig. I.1, where the normalized current I_N is defined by $I_N = I_p(MA)/a(m)B_t(T)$. The highest beta value, β~6.8%, was

obtained at I_N~2.5 and q_ψ~2.3 and a high beta state with g>2.4 was sustained for 0.7 s (Fig. I.2). The operational limit in current, I_N~3.2, corresponds to q_ψ~2. The beta limit obtained at q_ψ<2 is lower than the maximum value. The beta value at low q may be limited by energy confinement and available heating power[1] or it may be limited by MHD stability[see I.2.2]. For $I_N \leq 2.5$, and $\beta > 2.4 I_N$, a large amplitude n=2 mode appears , often preceded by an n=3 burst; this may cause the observed decrease in energy confinement time. A locked n=1 mode can also cause a beta collapse or disruption. Below $\beta = 2.4\ I_N$, a small amplitude n=2 mode and bursts of n=3 and 4 modes are observed without degradation of energy confinement.

The highest beta in a fully analyzed shot (shot number 55390) reached g=2.5 at I_N=2.5. For this case q_ψ~2.2. It was studied by using measured kinetic profiles of the electron density and temperature. The analysis shows that n=1, 2 and 3 ideal kink modes are stable without wall stabilization. The infinite n (ballooning) mode is calculated to be marginal at the inner region of the plasma and it is stable over most of outer volume (Fig. I.3). The measured electron density is almost flat near the magnetic axis. The q-profile in this case is inferred from measured kinetic profiles and magnetics analysis. It is found to be very flat in the central region, with a value near unity from the axis to the $\sqrt{v}=0.5$ point. The flux surface averaged current density profile is also found to be flat in the center, decreasing monotonically to zero near the edge.

The accessible high beta space in DIII-D shows a trend toward lower l_i (flatter j profiles) at high g (Fig. I.4). This trend is also seen in ideal, linear MHD analysis of the n=1 kink mode with wall at infinity and q_0~1. The experimental accessible stable region also narrows in g-l_i space at high g, suggesting that inability to maintain the highest g values in steady state may be due to relaxation of the current profile to a less stable form. It is also observed, however, that discharges with low l_i have a greater tendency to produce locked modes than those with high l_i.

DIII-D has obtained steady state low-q discharges in elongated configurations, reaching q_ψ~1.9 in an elongated single-null point divertor configuration with κ=2. For low-q, q_ψ<3,

τ_E/Ip is reduced by roughly 50% when q_ψ goes from 3 to 2 in H/D H-mode discharges (Fig. I.5). This may be due to large sawtooth radius, high frequency of edge localized modes (ELMs), and the large amplitude of these ELMs at low-q.

(2) JFT-2M [2]

The operational limit of H-mode discharges in JFT-2M was studied for B_t=0.65T, $2<q_\psi<3$, and neutral beam heating with $P_{heat}\leq$1.4MW. A maximum g-value of 2.5 was achieved with half of the maximum beam heating power. Strong saturation of energy confinement was observed above this power level. Combining ICRF with the neutral beams to extend the maximum available power did not help to increase beta. The g value obtained is lower than that for neutral beam heating alone. In most cases of ICRF heating the g value is limited below 2 (Fig. I.6). At higher B_t (B_t=1.2 - 1.5T) where the beta value is low, such strong saturation is not observed up to P_{heat}=1.4MW.

Shots with clear disruptions at the maximum beta are rare even at low q ($q_\psi<3$). Disruptions occur when B_t is lowered around g=2.5. They are similar to density limit disruptions.

(3) ASDEX [3,4]

The beta limit was studied in H-mode discharges for $1.2\leq B_t\leq 2.7$T, $0.2\leq I_p\leq 0.48$MA and neutral beam heating with $P_{heat}\leq$4.5MW. The operational beta limit is g_{max}=2.8 from diamagnetic measurements and corresponds to g~3.0 if the parallel beam component is included in the plasma pressure. Near this limit, beta collapse occurs. A nearly steady state is obtained for $g\leq 0.8g_{max}$. When $g>0.8g_{max}$, the high beta state is transient and the beta value decreases to g=2.2 after the peak value(Fig. I.7). Possible explanations are: a) a reduction in beta due to broadening of the current density profile caused by impurity accumulation in the plasma center during H-mode operation[3], b) direct reduction in the pressure at the plasma center due to intense local core radiation from these impurities (overall, $P_{rad}<P_{heat}/3$) [4].

The beta limit for $q_\psi\geq 3$ is usually non-disruptive. Disruption occurs during the transient phase when $q_\psi<3$.

(4) Summary of high beta experiments

A g-value, g=2.4-2.5 can be obtained for nearly steady state operation. For $2.5 \leq g \leq 2.7$, either a strong saturation in beta value (JFT-2M) or a beta collapse /disruption occurs(DIII-D and ASDEX) and higher beta, $g \geq 3$, can only be obtained transiently. It is not clear whether the transient profile can be sustained by a careful control of the profiles. The limits of I_N and q_J for high betas with $g \geq 2.4$ are summarized in Table.I.1 ($q_J \equiv 5(1+\kappa^2)a^2B_t/2RI_p$). The condition $q_J \geq 2$ appears to describe the limit for the plasma current in the experiments.

Table. I.1 q-limits in experiments

Device	A	κ	I_N^{max}*	q_J
DIII(NB)	4	1.6	1.1	2.0
PDX(NB)	3.2-4.0	1	0.6	2.1-2.6
PBX(NB)	4	2.0	1.5	2.1
ASDEX(NB)	4.1	1	0.5	2.3
JFT-2M(NB+IC)	4.3	1.5	1.0(0.8)**	1.9(2.4)
DIII-D(NB)	2.7	2.0	2.5	1.9

*I_N^{max} is the maximum normalized current above which disruption or serious beta degradation occurs.
**long duration with ELMs.

I.2.2 Theoretical prediction on beta and q-limits

Since there is no experimental data for $\kappa > 2$, only theoretical analysis is available to predict the beta limit in this case. Beta limits of elongated plasmas due to low-n kink ($n \leq 3$) and $n=\infty$ ballooning modes have been studied by using three cases of profiles;

Case 1[5] : $q=q_0+q_1\psi^{\alpha_1}+(q_\psi-q_0-q_1)\psi^6$,

$p=p_0[(1-\psi^{\beta_1})^{\beta_2}+p_1\psi^3(1-\psi)^{\beta_3}]$,

Case 2[6] : $q=q_0+0.5\psi^2+(q_\psi-q_0-0.5)\psi^6$,

or q-profile obtained from $Rj_\varphi=j_0(1-\psi^{\alpha_1})^{\alpha_2}$ at low beta,

p=optimized profile for ballooning mode with reduction near the plasma edge to stabilize kink modes ,

Case 3[7] : $\langle \mathbf{j}\cdot\mathbf{B}\rangle/\langle \mathbf{B}\cdot\nabla\varphi\rangle = j_0(1-\psi^{\alpha_1})^{\alpha_2}$,

p=optimized profile for ballooning mode
with smooth reduction for $0.8<\psi<1$,

where ψ is a normalized poloidal flux function for $0\leq\psi\leq1$. The safety factor at the magnetic axis, q_0, is chosen to be between 1.01 and 1.05 for the most of the cases to avoid local interchange modes. Cases with $q_0<1$ have been studied separately[8]. The plasma shape is specified by the formulae,

$$R=R_0+a\cos(\theta+\delta\sin\theta)$$

and

$$z=\kappa a\sin\theta \quad .$$

Equilibria are calculated in a fixed plasma boundary and q_ψ at the boundary is interpreted as the value at the 95% flux surface in a divertor configuration. The aspect ratio, $A=R_0/a$, is chosen about to be 3 for ITER.

Figure I.8 shows beta limits for A=3 (Profile cases 1 and 2) and 3.3 (Profile case 3) as a function of elongation, κ. The safety factor q_ψ is chosen as 3. For cases 1 and 2, there appears a maximum in beta. The corresponding value of κ depends on the choice of pressure profiles. Case 3 shows a monotonic increase of the beta limit with κ for $\kappa\leq2.5$. The envelope of the maximum points appears to give an almost constant beta limit for $2<\kappa<2.5$. For $\kappa>2.5$, the beta limit decreases mainly due to the external kink mode. It may be possible to enhance the beta limit for $2<\kappa<2.5$ by shaping and by careful optimization of the pressure and current density profiles. The g-limits for $q_\psi\geq3$ as a function of κ are shown in Fig. I.9. For $\kappa\leq2$, g takes values between 3 and 3.8 depending on the profile. The difference is mainly due to different profiles near the plasma edge. For $\kappa>2$, g decreases as κ increases. The average of the 3 cases gives

$$g=\begin{cases} 3.4 & \text{for } \kappa\leq2 \text{ and } q_\psi\geq3, \\ -9.12+12.3\kappa-3.02\kappa^2 & \text{for } 2\leq\kappa\leq2.5 \text{ and } q_\psi\geq3. \end{cases}$$

For $\kappa\geq2$, the g-limit due to external kink modes is insensitive to triangularity, δ, for $q_\psi\geq3$(Fig. I.10) and high magnetic shear (low current density) near the plasma edge. The beta limit can be increased if the plasma current increases as δ increases for a fixed q_ψ. However, the stability of internal modes strongly depends on δ when $q_0\leq1$[8]. Figure I.11 shows g-limit due to internal kink

modes as the function of δ for three different pressure profiles (Fig. I.11(a)). The g-limit increases as δ. A flat pressure profile near the axis is favorable to reach higher g (and β) (Fig. I.11(b)). This has been further demonstrated for profiles case 2 by adopting an optimization procedure in which the pressure gradient is required to vanish in the region $q(\psi)<1.1$[6]. As shown Fig. I.12, the profile with lower central q allows higher magnetic shear in the outer plasma region and larger pressure gradient can be supported there in comparison with the case $q_0=1.1$. Using this optimization technique the average beta value is increased for $q_0<1$ because of volume weighting effects.

Figure I.13 shows the dependence of g on q_J for case 1 profiles for a wide range of κ and δ. The range of constant g is limited by $q_J\sim1.8$ which is close to the experimentally obtained limit (see Table I.1). In experiments (e.g. in DIII-D), $q_J\sim1.8$ corresponds to $q_\psi\sim2.3$. However it corresponds to $q_\psi\sim3$ for some parameter sets of the case 1 equilibria with κ up to 2.5 and δ up to 0.5. The value q_ψ is sensitive to details in the q-profile near the plasma edge.

The beta limit is found to be quite sensitive to the assumed wall position for low q ($2<q_\psi<3$). The results of an analysis in this region, using profiles of the type in case 1 and ITER parameters ($A=2.9$, $2\leq\kappa\leq2.5$, $\delta=0.4$), are shown in Table I.2.

Table I.2 g-limits for low q

κ	g(wall at infinity)	g(wall at $a_w/a=1.5$)
2	< 1.8-2.3	< 3.6
2.25	< 2-2.4	< 3.8
2.5	< 2.5	< 3.3

The stability of high κ plasma is sensitive to the q-profile or current density profile (mainly near the edge), as indicated by the analysis of DIII-D experiments (Fig. I.4). The sensitivity is lowered for high edge shear. There is, however, less flexibility for obtaining large shear with q_0 constrained to be around unity and q_ψ to be near 2. The lower g-limits for low-q in Table I.2 reflect the fact. Figures I.14 and I.15 show the dependence of stable g on the maximum (edge) shear, $(dq/d\psi)/q$, for profile case1. Figure I.13 shows stable cases for $\kappa=2$ and Fig. I.15 those for $\kappa=2.5$. For

these calculations, A=2.9, δ=0.4 and $a_w/a = \infty$. Cases with q_ψ<3(crosses) are distinguished from those with q_ψ>3(squares). The κ=2.5 case shows that higher g can be obtained at low q than that for κ=2. A clear trend emerges from these low-q calculations indicating that increased g is correlated with sharply increasing shear near the edge through an increase in κ for a fixed current density or its derivative near the edge. This increase is mainly due to diminishing of "ravine" in the function $\beta(q_\psi)$ at q_ψ<3 where the stability of the kink modes is sensitive to the edge shear. In high-q, the dependence of stable g on κ is opposite as shown Fig. I.9. This trend is also indicated for profile case 3[7]. This degradation may be due to the mode coupling at central lower shear region and at outer high shear region.

The theoretical stable g values for low-q cases in ITER with wall at infinity are close to the stable values reported for DIII-D[1 and I.2.1], although DIII-D has a somewhat lower aspect ratio. The experimental results also suggest that the beta limit is sensitive to the magnetic shear (or the current density profile) and pressure derivative of the outer plasma volume. When the central current density or q_0 is limited by sawtooth oscillations, impurity accumulation or slow current penetration, the experimental current density and q-profiles become flat near the center and peaked near the plasma edge. For such profiles the marginal pressure derivative is small at the center and large near the edge. The limit of average beta can be large for these profiles because of the volume weighting effect.

For a given current profile, elongation and triangularity weaken the magnetic shear near the magnetic axis . In this region, the marginal pressure derivative for MHD modes becomes small and the peaking factor of the pressure, $\langle p^2\rangle/\langle p\rangle^2$, is about 1.2 for the optimized profile for ballooning, internal and external kink modes. If we assume the pressure profiles of the form, $p=p_0(1-\psi)^{2.2}$ and $p_0(1-\psi)^{1.5}$, the g-limit is reduced from 3.5 to 0.6 and 1.4, respectively, for case 1. The optimized pressure profile with g~3.5 is close to $p=p_0(1-\psi)^{0.7}$ except near the edge. (See Table I.3).

Table I.3 Peaking factor of pressure and g-value

P-profile	$\langle p^2\rangle/\langle p\rangle^2$	$p_0/\langle p\rangle$	g

$(1-\psi)^{2.2}$	2.25	4.0	≤0.6-0.9
$(1-\psi)^{1.5}$	1.6	2.9	≤1.4
$(1-\psi)^{\sim 0.7*}$	1.2	1.7	~3.5

*The exponent is fitted to the optimized pressure profiles to ballooning modes

I.3 Conclusions and Recommendations

I.3.1 Beta and q-limits

1) General conclusion

The ideal MHD theory predicts a maximum value of g, g_{max}=3-3.5. However this value is not a universal limit but depends on the plasma shape and profiles. The range where g is almost constant is given by $q_J=5(1+\kappa^2)a^2B_t/2RI_p \geq 1.8$ and $\kappa \leq 2.0$-2.2. ($q_\psi<3$ is in principle allowable but a more stringent q_ψ-limit is recommended, i.e. $q_\psi \geq 3$). It should be noted that these beta and g-values are obtained by ideal MHD calculations with optimized profiles of pressure and safety factor (or current density) for ballooning modes and low-n modes. Near the beta limit, resistive[10] and kinetic effects may be important.

In experiments, stable and nearly stationary operation was obtained with $g \leq 2.7$ (in DIII-D)[1], $g \leq 2.5$ (in JFT-2M)[2] and $g \leq 2.3$ (in ASDEX)[3,4]. In ASDEX, g can be 2.4 if the parallel beam pressure is included. The maximum value of g seems to be determined by current diffusion affected by impurity accumulation at the plasma center. In DIII-D large amplitude magnetic fluctuations were observed as g approaches 2.7 and beta collapse and/or disruption occurs for $g>2.7$, the maximum achievable g being 3.5. The corresponding q-limits are q_ψ~2.2, q_J~1.9 (DIII-D and JFT-2M) and q_ψ~3, q_J~2.3 (ASDEX) (see Table I.1). In DIII-D, operation in lower q (q_ψ~2) is possible with low beta, where the beta value is limited by energy confinement and available heating power. In ASDEX, beta limit for $q_\psi \geq 3$ is usually non-disruptive, whereas disruption occurs during a transient phase for $q_\psi<3$.

Assuming a relatively clean plasma and an elongation $\kappa \leq 2$, for performance predictions in ITER g=2.5 is recommended in the absence of efficient profile control

(which is the situation for ignition studies). For steady-state operation with the possibility of current profile control, g=3 is recommended. Optimistic projections to be covered as far as possible by the technical capability are g=3 for ignition studies and g=3.3 for steady-state operation.

2) Shape effect

In DIII-D, the maximum g is almost independent of κ, for $\kappa \leq 2$. There are no experimental data for $\kappa > 2$. Only ideal MHD analyses are available to predict the beta limit in this case[5-7]. An optimum shape, where the beta value takes its maximum, exists in $2 \leq \kappa \leq 2.5$. The optimum point in κ depends on the profiles and δ. The envelope of the optimum beta values, obtained for different profiles and δ, gives an almost constant beta limit for $\kappa \geq 2$ and moderate triangularity $\delta \leq 0.5$. At $\kappa \geq 2$, the triangularity plays an important role in the stability of the internal modes, e.g. at $\kappa=2$, the minimum δ needed to achieve an appreciable beta is ~0.4.

Studies in the range $2<A<4$ for $\kappa>1.6$ do not show a sizable dependence of g on aspect ratio. Further studies should be undertaken.

3)Profile effects

3.1) Safety factor

In the range $2<q_\psi<3$, stable discharges are possible but g may be small depending on the profiles and δ, because of external and internal kink modes becoming unstable. In addition, the energy confinement in this region is much affected by sawteeth. ITER should however have the technical capability to operate in this range. In this region the results are sensitive to assumptions about the conducting wall. The effect of plasma shape is also important. For performance predictions, $q_\psi \geq 3$ should be used. In the range $3<q_\psi<4$, theoretically g=3-3.5 is achievable for optimized profiles. However, as said above, stable and stationary discharges, in the experiments, are limited to $g \leq 2.5$. For $q_\psi>4$, a higher g may be possible and

the optimized profile tends to approach the experimentally observed profiles.

For q_0 <1, the possibility of an internal kink instability exists. When the radius of the q=1 surface exceeds half of the plasma radius, the beta limit decreases rapidly. If the pressure profile is flattened in $q(\psi)<1.1$ region, the higher beta limit can be increased due to the resulting higher shear in the plasma outer region and volume weighting effects. At large κ, triangularity is very beneficial to stabilize the internal kink instability through the increase in the edge shear[8]. However the compatibility with central heating such as alpha particle heating must be investigated.

3.2) Pressure profiles

For a given current profile, elongation and triangularity weaken the magnetic shear near the magnetic axis . In this region, the marginal pressure derivative for MHD modes becomes small and the peaking factor of the pressure, $<p^2>/<p>^2$, is about 1.2 for the optimized profile for ballooning, internal and external kink modes. The optimized pressure profile with g~3.5 is close to $p=p_0(1-\psi)^{0.7}$. A preliminary result suggests that the g-limit decreases as the peaking factor of the pressure increases. A peaked current profile is favorable for sustaining a peaked pressure profile near the plasma center to enhance the fusion power, although the total beta is less due to the reduction of the marginal pressure in outer portion of plasma.

3.3) Current density profiles

The optimization to current density profile has not been fully performed. In the analysis of experiments and in theoretical calculations, functional forms for the current density profile are assumed. The use of self consistent current profiles including the effect of classical or neoclassical resistivity, bootstrap current, or other current drive, and of sawtooth oscillations may be necessary.

I.3.2 Beta limit of fast alpha particles

Calculations have been done for circular cross section and simplified magnetic surfaces. The limit for the central beta of the fusion alpha-particles, due to the fishbone instability, is $\beta_\alpha(0)$~1-4%[9]. This implies that there is a limit on the central electron temperature, typically at $T_e(0)$~30keV. A higher value can be obtained if the magnetic shear near the axis is high. A stable window for the sawtooth and fishbone modes was found for a particular range of the amount of the trapped fast ion density[11]. The interaction of trapped energetic particles with kinetic ballooning modes has been studied for a non-circular cross section. A preliminary result shows an improved limit from finite Lamor radius effects.and a reduction of this limit due to alpha particles.

I.3.3 Possibility of a high κ equilibrium.

The possibility of evolving an equilibrium from a circular cross section up to κ=2.5 by changing the PF coil currents with was demonstrated in an MHD calculation. Up to κ=2.5 an intrinsic bifurcation of the MHD equilibrium has not been observed. The unstable eigenmode structure is close to a rigid displacement(m=1/n=0) as shown in the INTOR case with $\kappa \lesssim 2$. Feedback control of the radial position and of the plasma size was also demonstrated for κ=2 assuming up/down symmetry[12].

I.4 Future work on MHD limits

1. MHD beta limit

1.1) As described, the beta limit is very sensitive to assumed profiles, and the deterioration of the beta limit as the pressure profile becomes more peaked is a concern Further, the sensitivity of the maximum g to q (or current) profiles has been demonstrated, especially in the low-q region. Thus it is necessary to study the dependence of g on peaking factors and current density profiles. For this study, "realistic" current density profiles characteristic of those in present high-β experiments and in ITER scenarios and systems codes should be taken into account.

1.2) The same examination should be conducted for $q_0<1$.

1.3) The stability (beta limit) in the low-q ($q_\psi<3$) region deserves special attention. The results of an analysis in this region, using a class of pressure and current density profiles and ITER parameters (A=2.9, $2<\kappa<2.5$, $\delta=0.4$), are shown in Table I.2.

1.4) The ITER theoretical database contains results for A=2.5, 3.0, and 3.5. These results suggest that g does not vary much with A., but detailed dependence on κ and δ has not been studied for low-q. This dependence should be examined for $2.5<A<3.5$, to provide a database for present and future ITER design.

1.5).The dependence of the results on other ("realistic") current density profiles should be examined and comparison with experiments (if possible) is necessary. Attention should also be paid to the great sensitivity of q_ψ to geometry in divertor configurations, especially at low-q. The $q_\psi(95\%)$ for a given "current q" is sensitive to the current density or q-profile especially for large κ and δ:

$q_\psi(95\%)=2.2$-2.3 for $q_J=5a^2B_t(1+\kappa^2)/2RI_p\sim1.8$ in DIII-D,

$q_\psi(95\%)\sim3$ for $q_J\sim1.7$-1.8 in a fixed boundary equilibrium.

1.6) Experimental results on beta limits for non-NBI heating.
The experimental database for beta-limits is obtained only with NB heated discharges. It is important to assess the results for other heating methods.

2. $\beta_\alpha(0)$-limit

.Shaping effects on the stability limit due to fishbone modes may be important.. Also, the effect of magnetic shear and of the birth profile of alpha particles should be studied.

3. Effect of alpha particles on global beta limit

The effect of alpha particles on MHD modes (e.g. ballooning modes) should be evaluated for ITER parameters.

4. Effect of non-linearity and resistivity on tearing modes in shaped plasmas.

Ideal linear beta limits used for ITER guidelines must be checked with nonlinear and non-ideal computations. Results with nonlinear codes should be developed to follow the nonlinear evolution of 'infernal' modes arising for low shear. The optimal ideal MHD profiles have high shear near the edge. Thus, resistive tearing calculations should be pursued in shaped plasmas to explore the compatibility of these profiles with those arising from possible mode saturation at high-beta. If a saturated state is found, the degree to which magnetic islands lie within the separatrix surface is an important matter to be investigated.

5. Effect of $p_{//} \neq p_{\perp}$ for technology phase

In the low density current driven technology phase, there will be significant non-inductive current, an anisotropic pressure profile, and possibly significant toroidal rotation. These effects will modify the poloidal field magnetics and the beta limits.

5.1) The modification of flux surfaces by anisotropic pressure should be estimated

5.2) The beta limit dependence should be checked for profiles typical of CD applications, as these are developed.

5.3) A preliminary estimate of the effect of toroidal rotation and pressure anisotropy on PF magnetics should be developed.

References

[1] E. J. Strait, "Stability and Operational Limits in DIII-D," ITER Specialists' Meeting on Operational Limits, 6-10 June 1988, Garching.

[2] H. Matsumoto, "Operational Limits in JFT-2M," ibid.

[3] INTOR Group, International Tokamak Reactor, Phase Two A Part III (Rep. Int. Tokamak Reactor Workshop, Vienna, 1986-87), IAEA, Vienna (1988).

[4] O. Gruber, "Energy Confinement and MHD Stability in ASDEX near the Beta Limit," ITER Specialists' Meeting on Operational Limits, 6-10 June 1988, Garching.

[5] J. T. Hogan, "Linear Ideal MHD Stability Calculations for ITER," ibid.

[6] L. M. Degtyarev et al., "Linear Ideal MHD Beta Limits in Tokamak," ibid.
Supplement to the report on the ITER Specialists' Meeting on Operational Limits (June 6-10, 1988, Garching, FRG).

[7] M.W. Phillips, "Effect of Shaping on the Stability of High Current, High Beta Tokamaks," ibid.

[8] J. Manickam, "Internal Kink Modes and the Importance of Profile Shaping in ITER," ibid.

[9] H. E. Mynick, "Alpha Confinement in ITER," ibid.

[10] D. Correa-Restrepo, "Resistive Ballooning Modes in INTOR," European Contributions to INTOR Phase Two A Part 3, EURFUBRU/XII-139/88/EDV1, Vol. II,IV-43 (1988).

[11] R.B. White, M. N. Bussac, F. Romanelli, "High Beta, Sawtooth-Free Tokamak Operation Using Energetic Trapped Particles," ibid.

[12] L. D. Pearlstein and T. B. Kaiser, "ITER Equilibrium, Stability and Ramp-up Simulation," ibid.

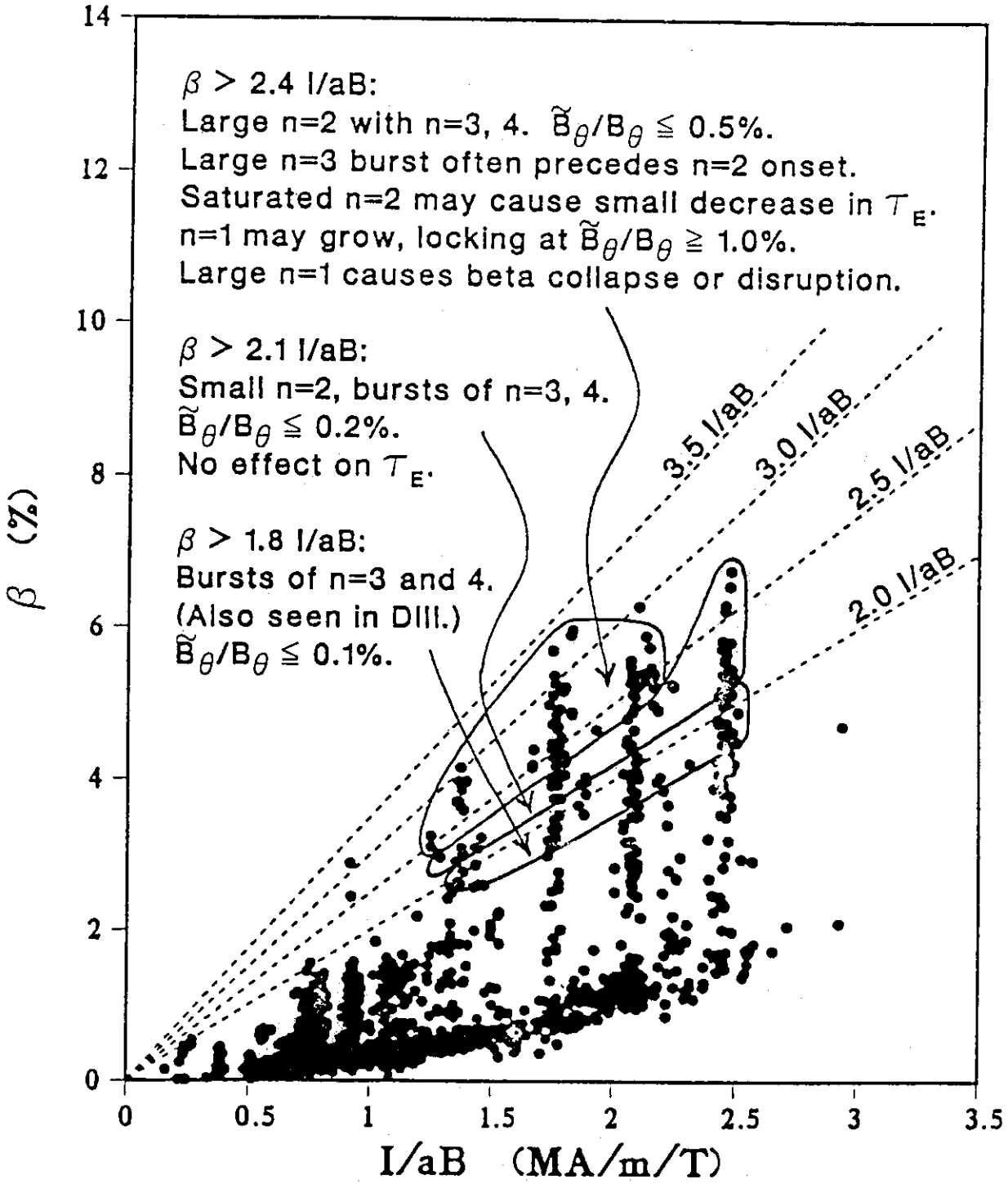

Fig. I.1 ß vs. I_N in DIII-D tokamak. As g increases, MHD instabilities appear. For g>2.4-2.7, large amplitude low-n modes cause beta collapse and disruption. The limit of I_N is 2.5 which corresponds to q_ψ=2.2-2.3. Above I_N=2.5, the beta value is limited by poor energy confinement and the available heating power [1]

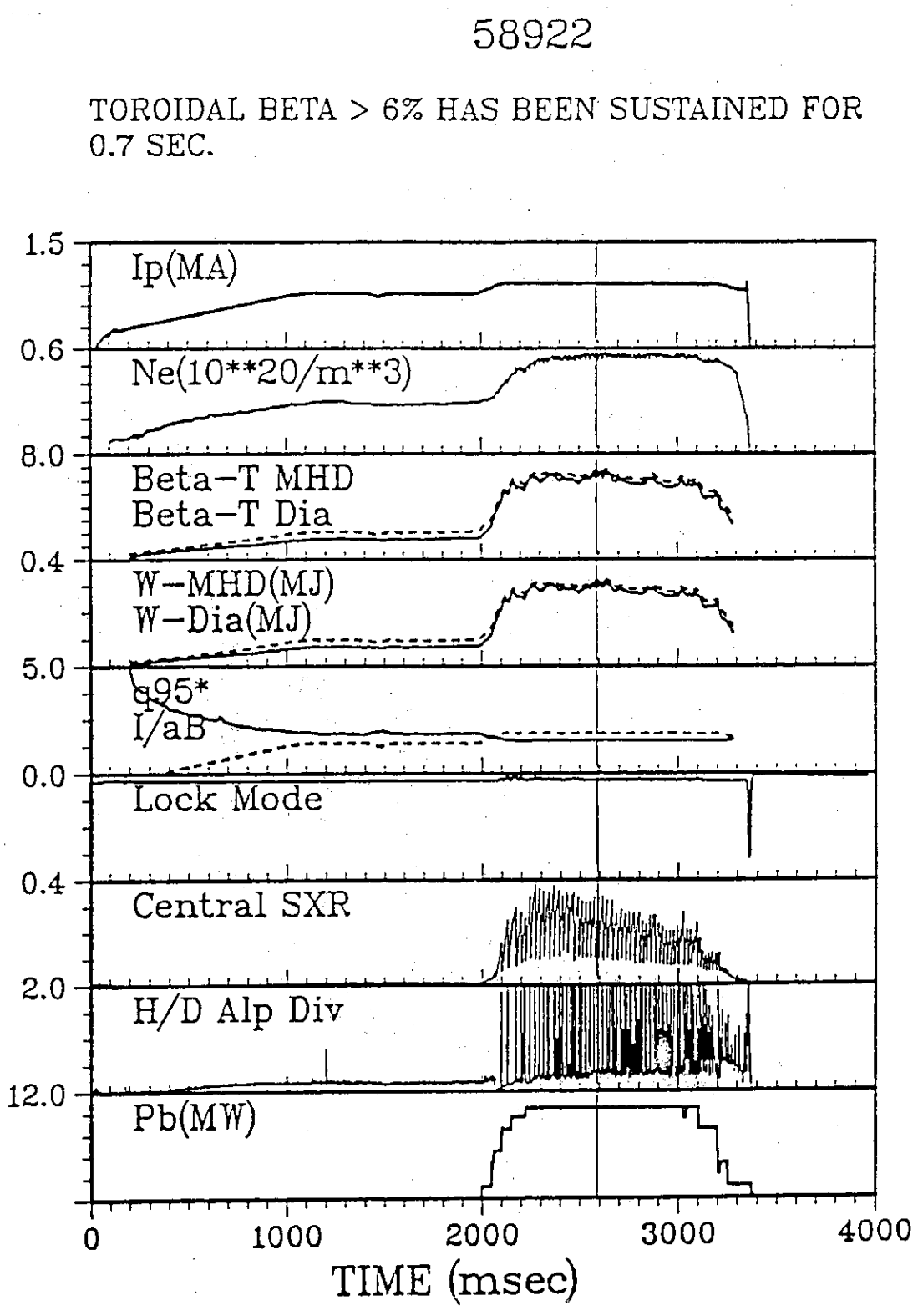

Fig. I.2 Nearly steady state of high beta discharge in DIII-D for $q_\psi \sim 2.3$. Beta>6% (g>2.4) is sustained for 0.7 s [1].

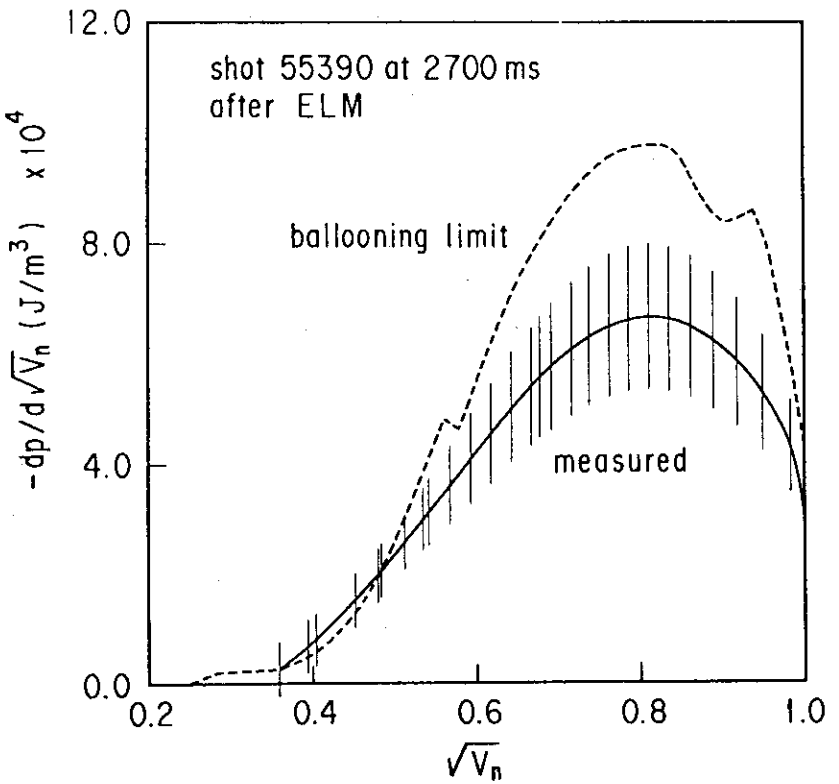

Fig. I.3 Measured pressure derivative and marginal p' for ballooning modes in DIII-D tokamak. The current density profile is obtained from magnetic measurements and from the measured kinetic profiles of electron density and temperature. Low-n modes ($n \leq 3$) are stable and ballooning modes are stable over most of outer plasma volume [1].

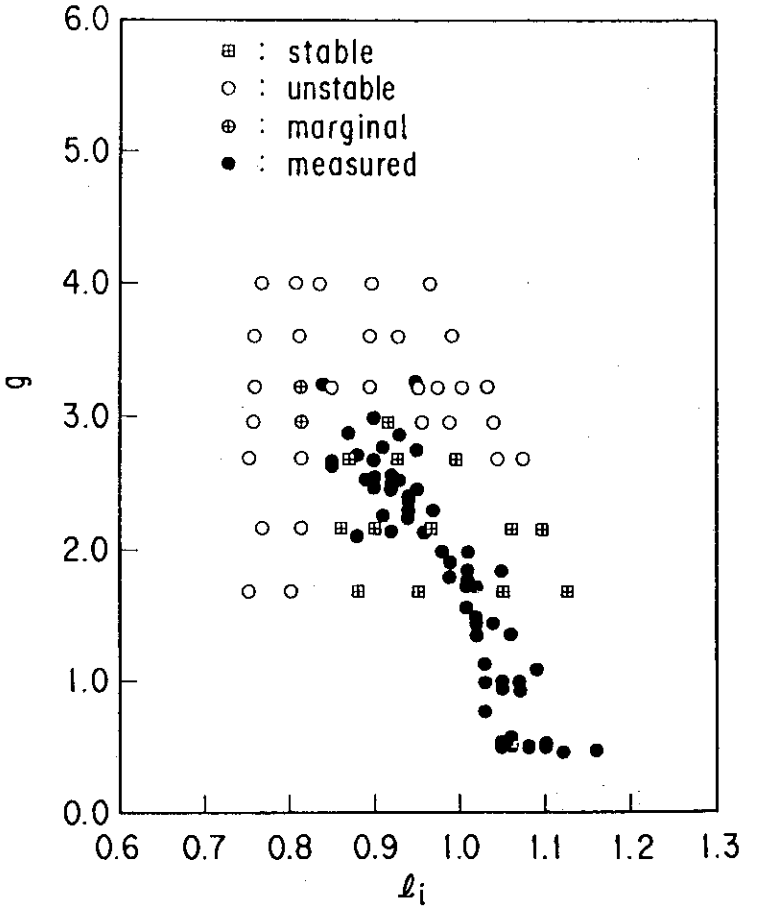

Fig. I.4 Operational range in g-l_i of DIII-D for q_ψ=3.2. Closed circles are measured points and others are obtained by the kink mode stability. The high g (g>3) can be obtained in narrow region of l_i[1].

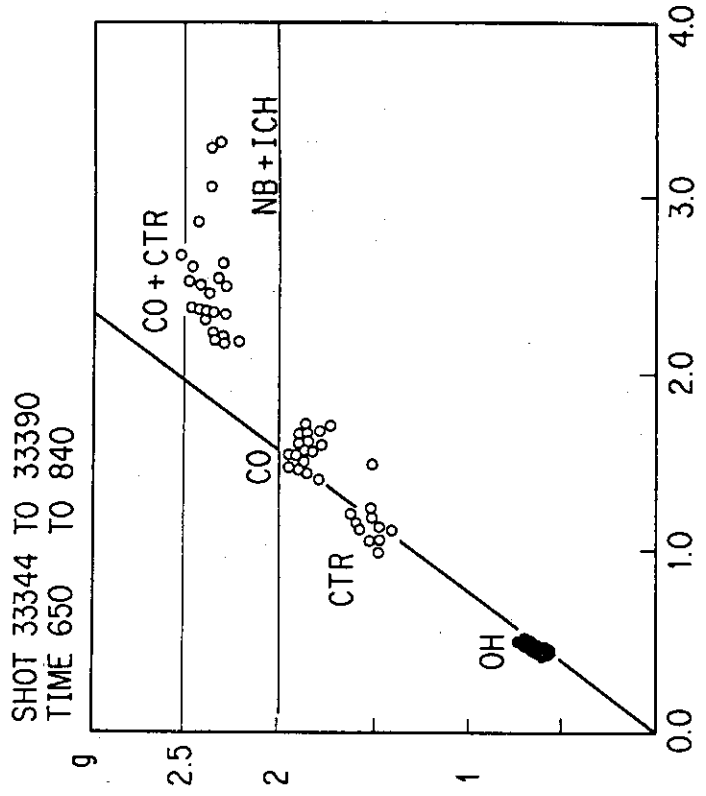

Fig. I.6 g vs. heating power in the JFT-2M tokamak. The g-value is limited to g=2.5. For the combination of neutral beam and ICRF heating the g value is limited to g^2 for most cases [2].

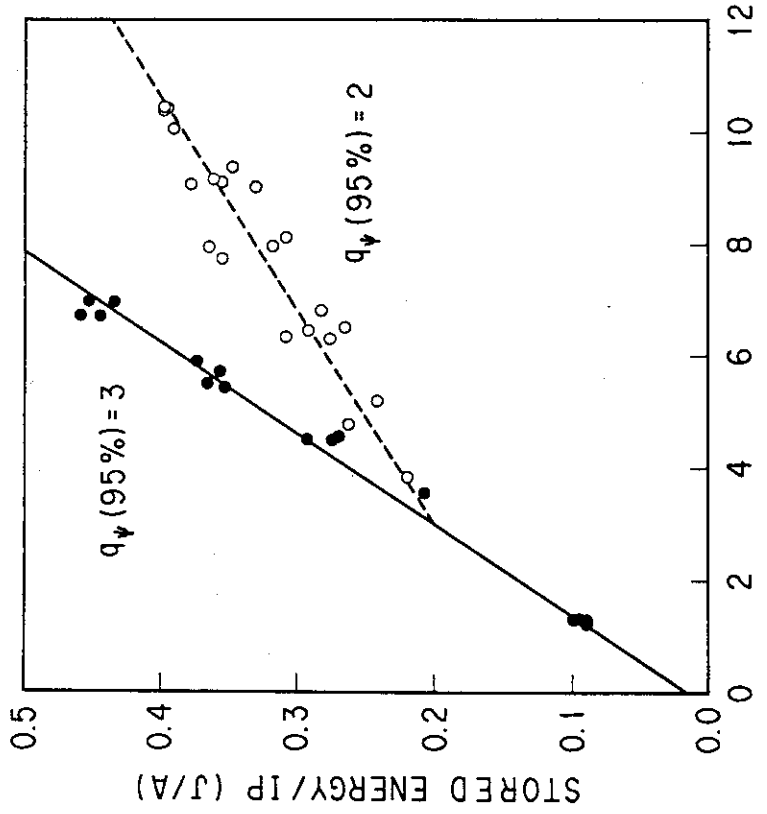

Fig. I.5 Stored energy/I_p vs. heating power in DIII-D. τ_E/I_p decreases for low-q. This may be due to the large q=1 radius (r/a^0.5), the high ELM frequency and the large depth of ELM observed in low-q discharge [1].

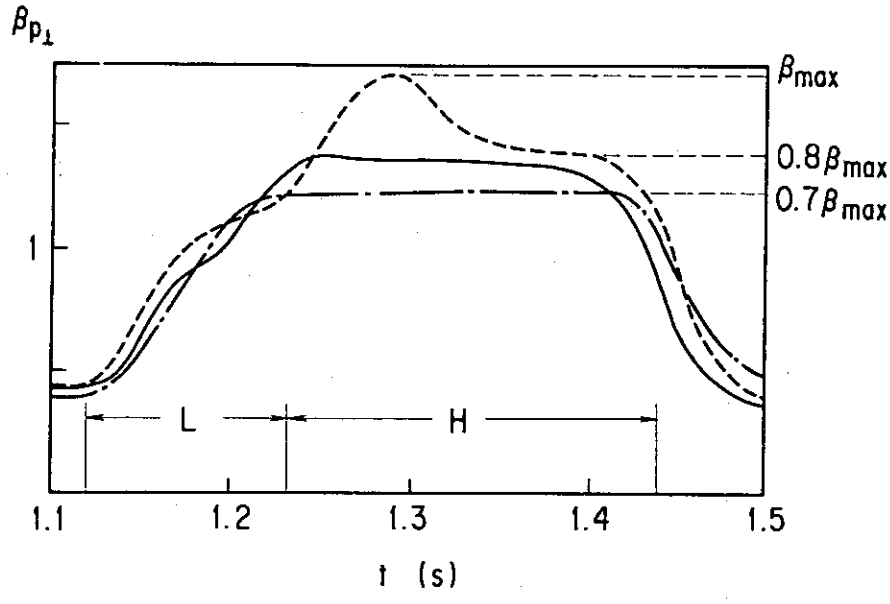

Fig. I.7 Time evolution of poloidal beta value in ASDEX. For g>2.2 (from diamagnetic measurement), beta collapse occurs [4].

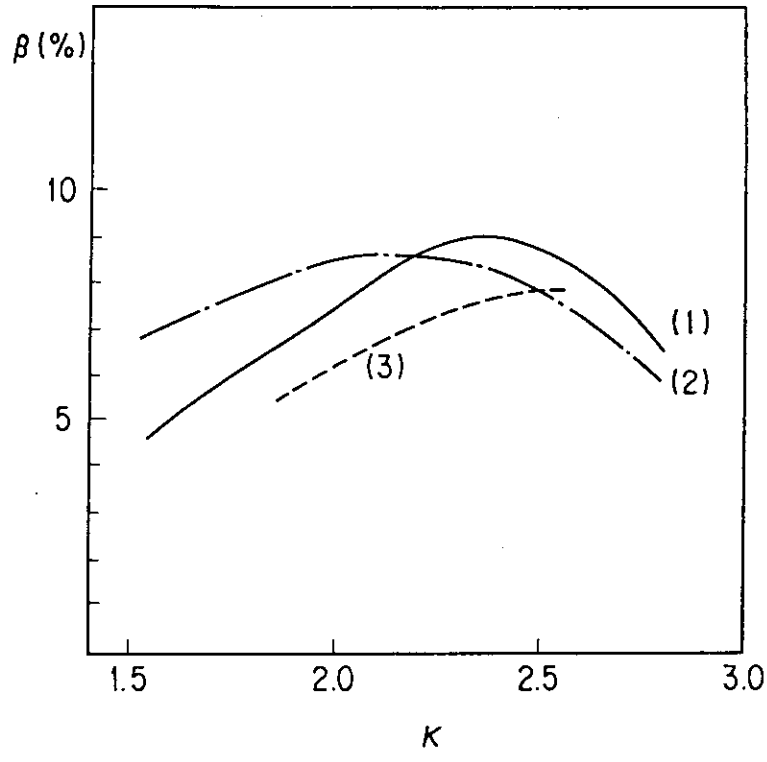

Fig. I.8 ß vs. κ for $q_\psi \sim 3$. The curves (1), (2) and (3) denote the profile cases 1, 2 and 3. For cases 1 and 2, the aspect ratio is A=3. A=3.3 for case 3. The envelope of beta limits for different equilibria gives an almost constant limit for $2<\kappa<2.5$.

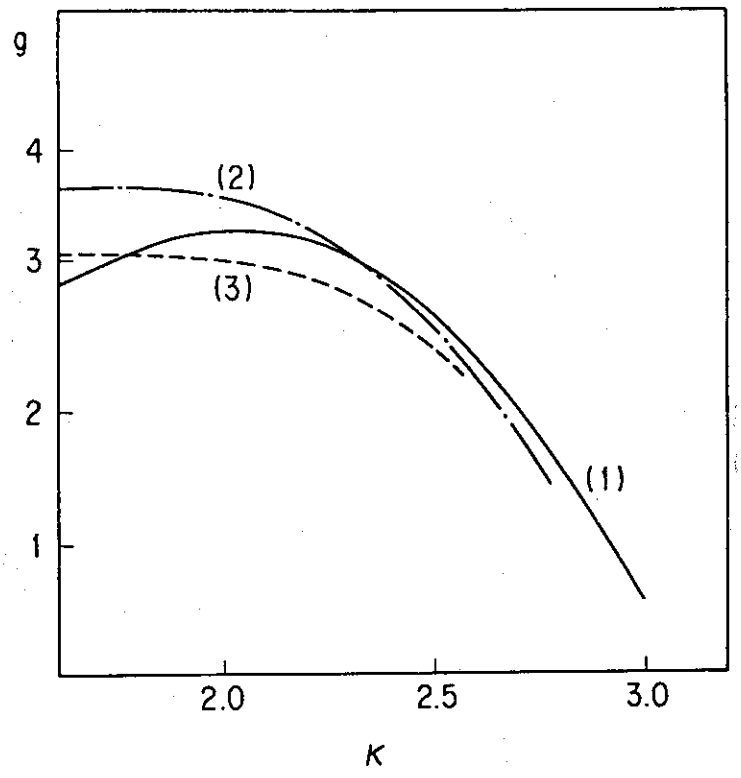

Fig. I.9 g vs. κ for $q_\psi \geq 3$. The curves (1), (2) and (3) denote the profile cases 1, 2 and 3. For $\kappa \leq 2$, g reaches about an average value of 3.4 and decreases for $\kappa > 2$.

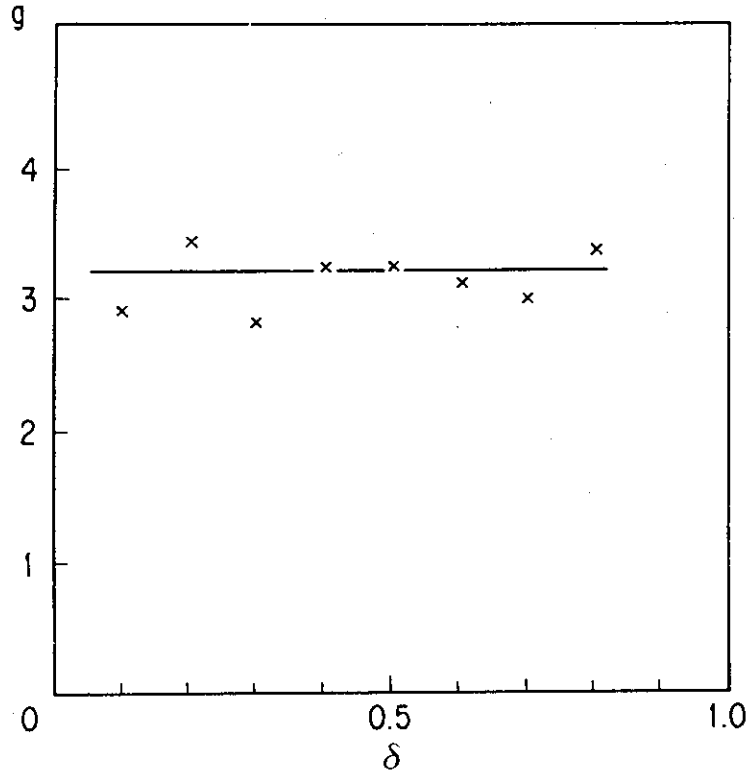

Fig. I.10 g vs δ for κ=2 and $q_\psi \geq 3$. The g-limit is insensitive to δ [5].

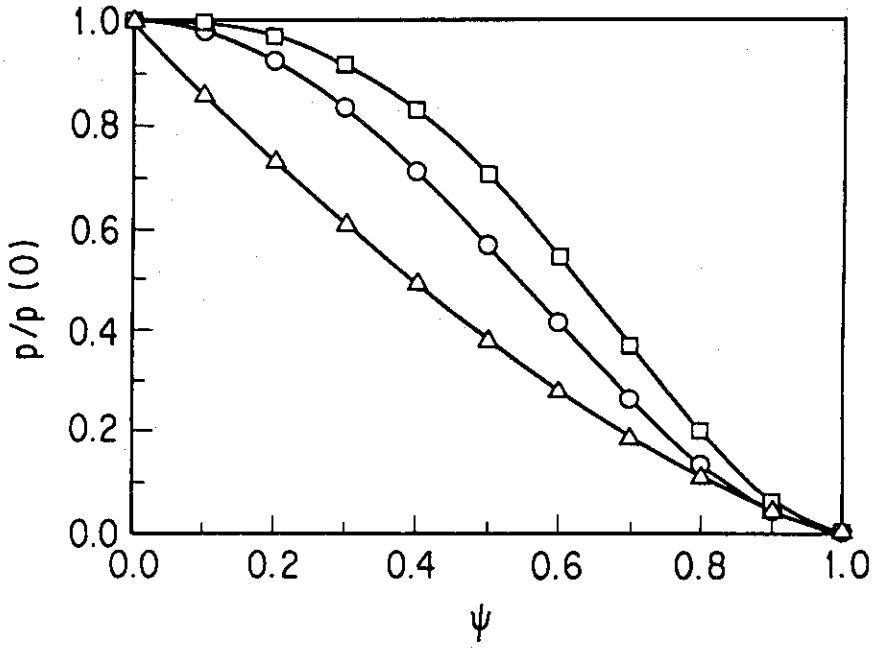

Fig. I.11(a) Pressure profile used for the analysis of internal kink modes.

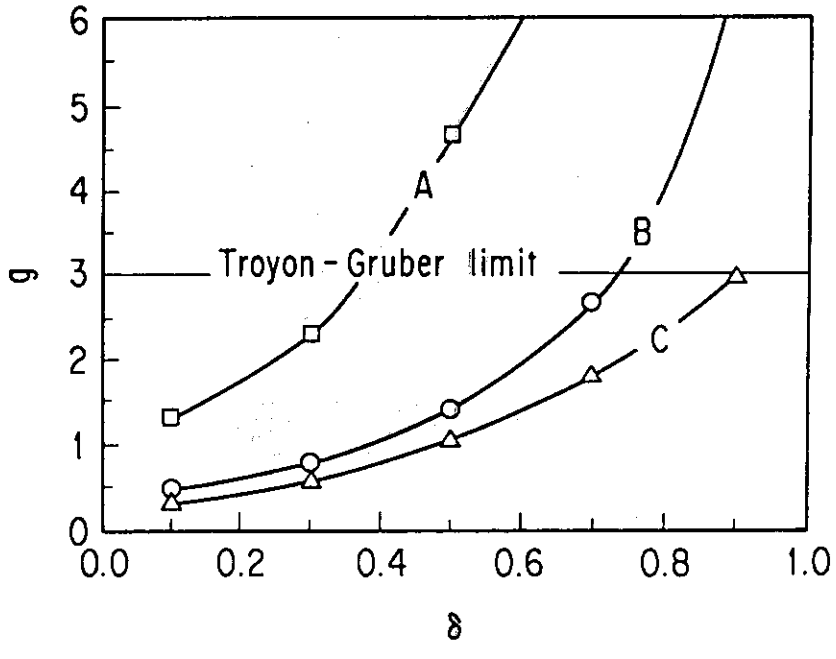

Fig. I.11(b) g vs. δ. The symbols correspond to those in Fig. I.11(a). A flat pressure profile is favorable to reach high beta [8].

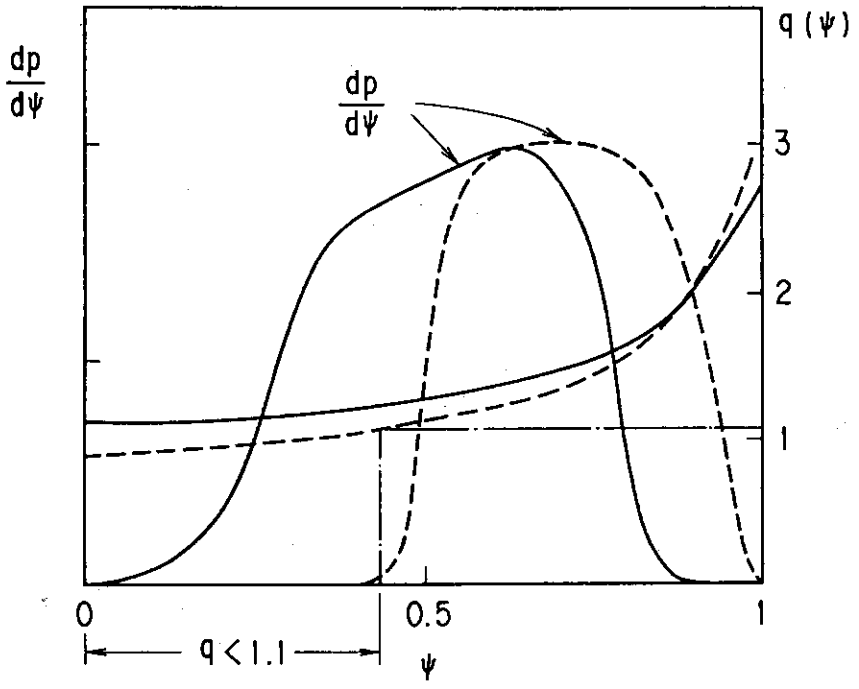

Fig. I.12 Comparison using profile case 2 of cases with q_0=1.1 (solid) and 0.9 (dashed). The pressure gradient $dP/d\psi$ is made to vanish for $q(\psi)$<1.1 for q_0=0.9 case. A higher pressure gradient can be supported in the outer plasma region.

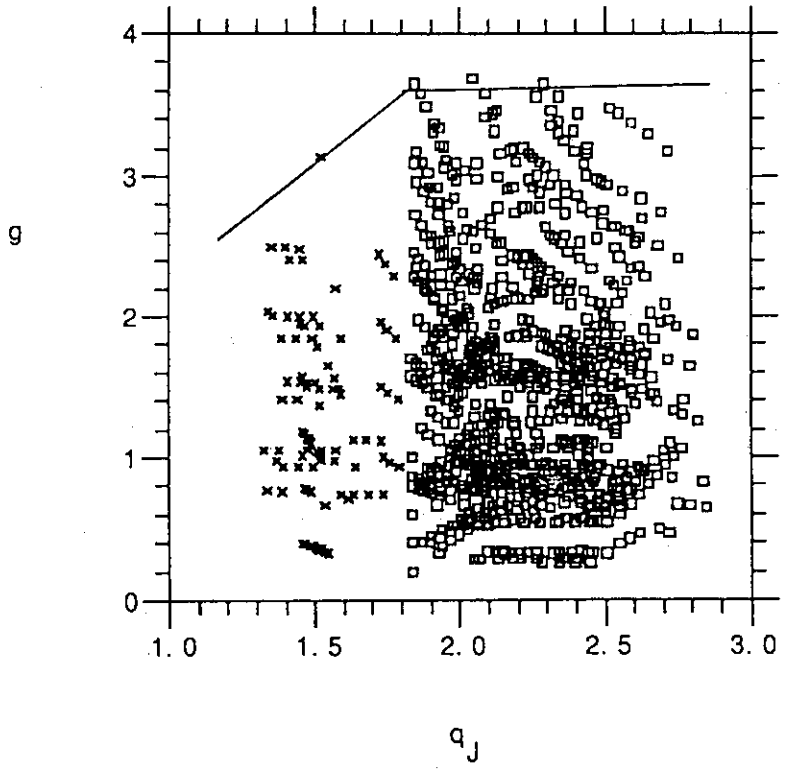

Fig. I.13 g vs. q_J for profile case 1. The square and cross symbols denote cases for $q_\psi \geq 3$ and $q_\psi < 3$, respectively. The maximum g-value is almost constant ($\sim$3.5) for $q_J \geq 1.8$.

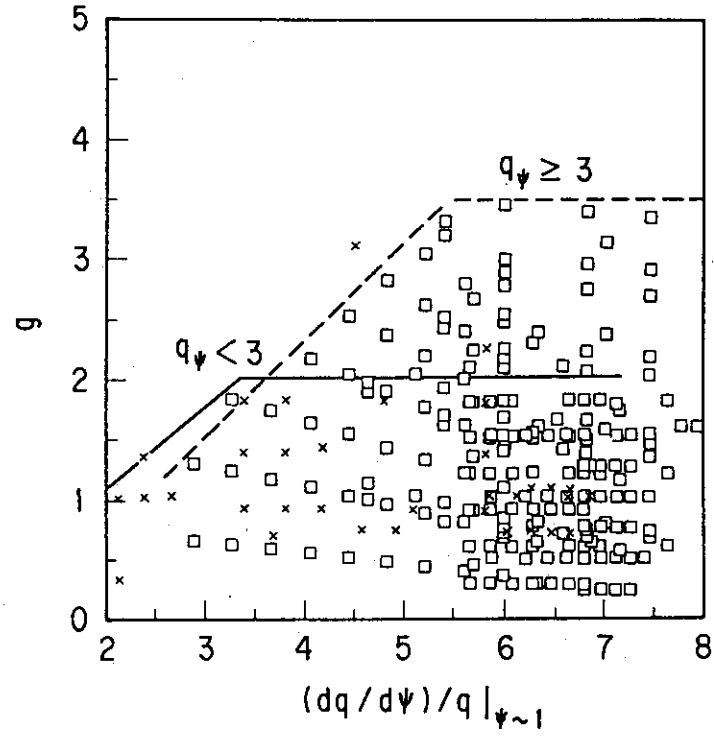

Fig. I.14 g vs. magnetic shear, $(dq/d\psi)/q$ at the plasma edge for κ=2. The stable g value for low-q is smaller than that for high-q.

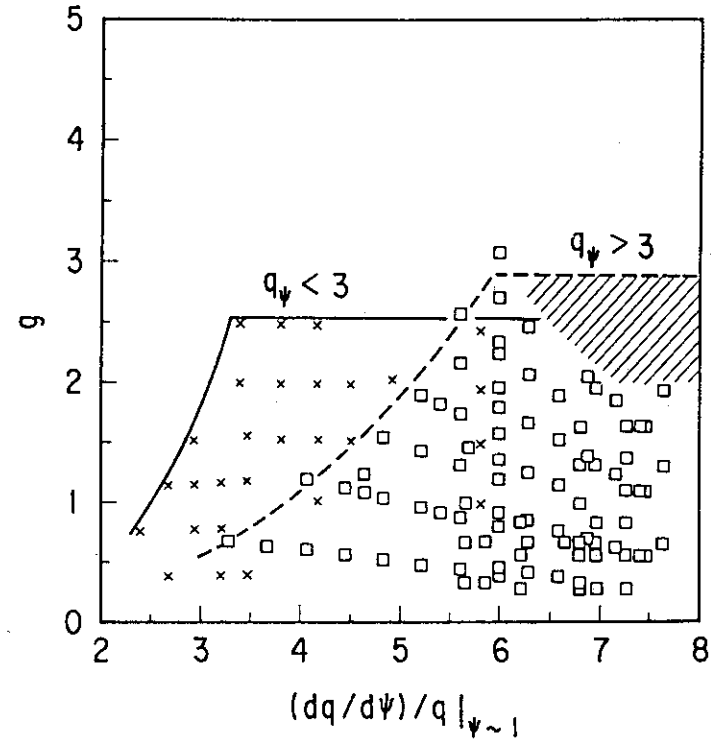

Fig. I.15 g vs. magnetic shear, $(dq/d\psi)/q$ at the plasma edge for κ=2.5. The g-limit for low-q increases. This trend is opposite to high-q cases.

Ⅱ. Density Limit

II.1 General Picture

A widely accepted picture of the general mechanism that triggers high-density disruptions and thus determines the density limit has evolved. In this picture cooling of the plasma edge leads to shrinking of the current channel, which destabilizes the $m/n = 2/1$ tearing mode when the $q_\psi = 2$ surface is reached. In principle, a variety of mechanisms may cause edge cooling. Besides impurity radiation, charge exchange and ionization losses as well as anomalous heat conduction may be important. Particle transport may have an indirect impact as it effects the plasma density at the edge and because of its importance in determining recycling. Recently, two different views of the density limit have been developed by M. Greenwald et al. [1] and F. C. Schüller [2] [3] which emphasize the roles of particle transport and edge impurity radiation, respectively. Both give a quite coherent interpretation of many of the available data and provide a tentative basis for extrapolation to ITER. Other studies were performed more or less along one of these two lines and are discussed in this frame. An explanation of the density limit which is based on anomalous edge heat conduction was also presented and used to interpret density-limit observations in T-10.

II.2 Greenwald Model

Greenwald's analysis refers to the general shape of the tokamak operation space in the $1/q$-$n_e R/B_t$-space as shown in Fig. 1. Mainly the lower bound is addressed, while the right bound, following the original ideas of Murakami, is interpreted as a radiative limit. On the basis of Alcator C pellet refuelling experiments, which show strong reduction of the density decay time near the density limit (see Fig. 2), it is concluded that this degradation of particle confinement is the driving mechanism for the appearance of the n-limit. Loss of particle confinement induces stronger recycling/refuelling which leads to increased charge exchange and radiation losses.

On the basis of data from Alcator C, Doublet III and PBX a quantitative expression for the n-limit is given:

$$\langle n_e \rangle^{crit} = \alpha \kappa J \qquad (1)$$

$(10^{20} m^{-3}; MAm^{-2})$, where $\langle n_e \rangle$ is the line averaged electron density, κ the elonga-

tion and J the mean plasma current density; $\alpha \simeq 1$ is claimed to hold independently of the heating mechanism or refuelling method. Apart from the beneficial dependence of elongation eq.(1) is essentially identical to the classical Hugill limit. It is of a purely empirical nature and not directly related to the physical picture outlined above. The latter is used to give a qualititative explanation of some observations which, at first glance, seem to contradict the Greenwald limit.

In Greenwald's interpretation the fuelling method plays a central role. Central fuelling requires a weaker particle source to maintain the density and this is taken as an explanation of the improved n-limit in pellet-refuelled discharges. Also the improvement by additional heating, which has been mainly studied in neutral beam heated plasmas, is considered to be due to the central fuelling by beam injection. This argument is used in particular to explain the difference in behaviour between beam-heated discharges and discharges with ICRH in JET [4].

JFT-2M density limit studies were reported which were analyzed with a special view to a possible impact of elongation [5]. In ohmic plasmas with $1 \leq \kappa \leq 1.5$ no clear dependence of the critical density on elongation is observed. The Hugill limit gives a slightly better fit than the Greenwald limit. No points above either the Hugill limit or the Greenwald limit have been found. In H-mode discharges the density limit is not disruptive but is rather given by the maximum density for which H-mode operation is possible. At this limit transition into the L-mode occurs.

II.3 JET Model

The Schüller model emphasizes the role of radiation and is based on the following observations which are generally made in JET high-density disruptions:

i) $P_{rad} = P_{in}$ holds at the limit, where P_{in} is the total input power and P_{rad} is the radiated power, which is predominantly emitted from the plasma periphery.

ii) The radiation mantle grows inwards and the disruption occurs when the this mantle reaches the $q_\psi = 2$ surface.

Observations i) and ii) lead to the following threshold condition for the occurance of an n-limit disruption [2] :

$$P_{in} = \int_2^{q_a} \Phi_{rad}(q') \frac{\partial V}{\partial q'} dq' = \bar{\Phi}_{rad}(q = 2/q_a) V(q = 2/q_a) \ , \qquad (2)$$

where $\bar{\Phi}_{rad}$ is the mean power density radiated from the volume $V(q = 2/q_a)$ enclosed by the $q_\psi = 2$ surface and the plasma boundary. Making the assumption that all profiles depend at most on q_a, one has

$$\bar{\Phi}_{rad} \simeq \langle n_e \rangle^2 (q = 2/q_a) f_1(q_a, Z_{eff}) \ , \qquad (3)$$

$$\langle n_e\rangle(q=2/q_a)/\langle n_e\rangle \simeq f_2(q_a) \tag{4}$$

and

$$V(q=2/q_a) \simeq 2\pi^2 Rabf_3(q_a)\ , \tag{5}$$

which immediately leads to the following general scaling of the density limit:

$$\langle n_e\rangle^{crit} \sim \sqrt{\frac{P_{in}}{Rab}\, g(q_a, Z_{eff})}\ . \tag{6}$$

Here Z_{eff} in f_1 is to be taken as a label for the impurity content, while q_a labels the q-profile. Of course one would expect g to differ for different configurations (limiter/divertor configuration), different discharge modes (L-/H-mode) and different boundary conditions (gas puff/pellet injection). In pellet-refuelled discharges, for instance, f_2 decreases and $\langle n_e\rangle^{crit}$ should increase in agreement with experimental observations. The decrease/increase of $\langle n_e\rangle^{crit}$ during current ramp-up/down is explained by an increase/decrease of f_3, respectively. The difference between beam-heated JET discharges and those with ICRH is interpreted in this picture as a consequence of the different impurity levels [4] (change of f_1). On the other hand, the power (density) scaling of $\langle n_e\rangle^{crit}$ and the lack of any other dependence except on q and on the impurity content should be device-independent.

The natural extension to divertor configurations would be to replace $V(q=2/q_a)$ by the volume enclosed by the q_ψ surface and the separatrix. In that case q_a has to be replaced by another label of the q-profile, such as q_I $(=\frac{2\pi}{\mu_0}\frac{B_t a^2}{I_p R_0}\frac{1+\epsilon^2}{2})$.

Making model assumptions about f_1, f_2 and f_3 allows to cast eq.(6) in a more specific form [2] :

$$\langle n_e\rangle^{crit} \simeq 2.5\cdot 10^{10}\sqrt{\frac{P_{in}}{Rab}\frac{1}{(Z_{eff}-1)}\frac{q_I^{1.5}}{q_I-2a/b}} \tag{7}$$

(n in m^{-3}; P in MW; R, a and b in m) Equation (7) is a good description of the density limit in gas-puffed JET limiter discharges in the parameter ranges $Z_{eff} > 1.5$, $q_I > 2.5$ and $1.2 < b/a < 1.6$, in which the model assumptions made are valid.

The role of radiation is not unique in this picture. Obviously the model breaks down in very clean plasmas, as is also indicated by the Z_{eff}-dependence in eq.(7) . A natural extension to that case would be the inclusion of charge exchange losses in eq.(1).

The power scaling as exhibited by eq.(6) should be a relatively general feature if the density limit is radiative. It has been well confirmed by old ASDEX data which

were obtained before the hardening of ASDEX [6]. Recent ASDEX measurements, performed after the hardening of ASDEX, show, however, a much weaker power dependence of $\langle n_e \rangle^{crit}$ [6], but under the same conditions (q, B_t, P_{in}) higher critical densities are achieved. In these discharges $Z_{eff} \simeq 1.2$ and the results may be indicative of a different mechanism, such as charge exchange losses, which may dominate over radiation losses in these clean discharges. This point is not yet fully understood. It is noteworthy that the best ASDEX points are close to, but still below the Greenwald limit (see Fig. 3).

In this context the old DITE results [7], which were the basis for the formulation of the Hugill limit, also have to be mentioned. They show, more in agreement with the Greenwald picture, a shift of the right boundary of the operation space (see Fig. 1) in the presence of additional heating, while the lower boundary is unaffected.

The physics underlying the radiative collapse is relatively simple and offers the possibility of a theoretical description by advanced transport codes. A study of this kind using the 1 1/2-D BALDUR transport code has been started [8] [9]. Critical issues of this approach are the proper description of a disruption condition, the impurity description in the boundary region and the modelling of radiation losses. In fact, coronal models, typically used in transport codes, strongly understimate the radiation in actual experiments [10]. The general features of a radiative limit are reproduced, but further code refinement is required for a quantitative description. Such models may provide an efficient tool for detailed analysis of experimental data.

II.4 T-10 Model

An interpretation of T-10 data was given in terms of a model which, under typical discharge conditions, leads to strong peripheral heat conduction and diffusion [11]:

$$\chi_e = \chi_e^I + \chi_e^{II} \simeq \frac{c^2}{\omega_{p,e}^2}(\varepsilon \frac{v_e}{qR} + \nu_{ei}) \ ,$$

$$D \simeq \chi_e \ ,$$

$$\chi_i \simeq \chi_e \ . \qquad (8)$$

The first term gives a scaling of the neo-Alcator type. For the second term $\chi_e^{II} \sim T_e^{-3/2}$ holds, leading to a strong increase of χ_e^{II} at the edge. Numerical studies of ohmic discharges for T-10 parameters, based on this transport model, were reported [11]. They show a sharp T_e drop at the plasma boundary if n_e is increased beyond a certain threshold value (see Fig. 4). For ohmic discharges the scaling $\langle n_e \rangle^{crit} \sim I_p$

seems to be reproduced. The model also describes the sharp decrease of the density decay time in pellet-refuelled T-10 discharges at densities close to the critical density.

II.5 Discussion and Implications for ITER

Cooling of the plasma edge being the essential triggering mechanism for high-n disruptions is now widely accepted. The various views of the density limit that were reported essentially differ in the underlying edge cooling mechanism. All are supported by some experimental evidence, typically obtained in one device. In all cases, however, conflicting results from other machines or different discharge conditions can be identified. The most obvious explanation is that the density limit is a multi-regime phenomenon and that one is faced with different regimes in different devices and sometimes even in one device if the discharge conditions are changed. An extrapolation to ITER conditions is difficult in this situation.

As a consequence of the general picture two necessary conditions for safe operation follow, which should be adopted as guidelines for ITER:

i) The power radiated from the plasma edge should be a sufficiently small fraction of the power flux to the edge region ($total\ power - bulk\ radiated\ power$).

ii) $q_\psi(95\%)$ should be sufficiently high in order that the distance between the $q_\psi = 2$ surface and the separatrix be not too small.

Whether this is sufficient and how it translates into a critical density is, however, unclear. The critical densities as predicted by the various versions of the density limit which exist in explicit form are summarized in Table 1 for parameters which are representative of ITER in the ignited mode of operation ($a = 2m; R = 5.8m; I = 20MA; s = b/a = 2; B_t = 5.1T; T \simeq 10keV; P_f = 1000MW$)

Table 1 Predected density limit of ITER

$\langle n_e \rangle$	operation density (line averaged)	$1.65 \cdot 10^{20}$	(m^{-3})
$\langle n_e \rangle_H^{crit}$	Hugill limit[a)]	$7.6 \cdot 10^{19}$	(m^{-3})
$\langle n_e \rangle_G^{crit}$	Greenwald limit	$1.5 \cdot 10^{20}$	(m^{-3})
$\langle n_e \rangle_{Sch}^{crit}$	Schüller limit according to eq.(7)	$8.7 \cdot 10^{19}$	(m^{-3})
$\langle n_e \rangle_{rad}^{crit}$	JET ohmic[b)]+eq.(6)	$1.4 \cdot 10^{20}$	(m^{-3})

a) $\langle n_e \rangle^{crit} \simeq 1.0J \quad (10^{20} m^{-3}; MAm^{-2})$

b) $\langle n_e \rangle^{crit} \simeq 0.5J \quad (10^{20} m^{-3}; MAm^{-2})$

Application of eq.(7) is not really justified in a divertor configuration and $\langle n_e \rangle_{Sch}^{crit}$ is only given for completeness; $\langle n_e \rangle_{rad}^{crit}$ is based on the JET ohmic limit and the power scaling according to eq.(6) . An estimated value of 10 MW for the ohmic power was used. The radiative limit should at least provide an upper limit for the actual n_e^{crit}. It is noteworthy that this limit, when estimated on the basis of JET ohmic operation and eq.(6) , would only be marginally sufficient to allow for generating 1000 MW in ITER for the assumed parameter set. On the other hand, in a clean plasma ($Z_{eff} \simeq 2$) under ITER working conditions still higher densities result to be accessible.

References

[1] M. Greenwald et al., A New Look at Density Limits in Tokamaks, MIT Plasma Fusion Center Report No. PFC/JA-86-22, January 1988

[2] F. C. Schüller, Operational Aspects of JET Disruptions, talk given at the "IAEA Technical Committee Meeting on Density Limit and Disruptions", JET Joint Undertaking, 26-28 January 1988

[3] F. C. Schüller et al., Experimental Observations of Disruptions in JET, 12th European Conference on Controlled Fusion and Plasma Physics, Budapest, 1985

[4] D. J. Campbell et al., Sawteeth and Disruptions in JET, Plasma Physics and Controlled Nuclear Fusion Research 1986, Vol. 1, 433-445

[5] Japanese Contributions to the ITER Specialists Meeting on Operational Limits, June 6-10, 1988

[6] EC Contributions to the ITER Specialists Meeting on Operational Limits, June 6-10, 1988

[7] P. E. Stott, J. Hugill, S. J. Fielding et al., Proceedings of the 8th European Conference on Controlled Fusion and Plasma Physics, Prague 1979, Vol. 1, 151

[8] D. P. Stotler, Transport Simulation of a Density Limit in Radiation-dominated Tokamak Discharges - Profile Effects, PPPL 2531, May 1988

[9] US Contributions to the ITER Specialists Meeting on Operational Limits, June 6-10, 1988

[10] K. Behringer et al., Plasma Physics and Controlled Nuclear Fusion Research 1986, Vol. 1, p. 197

[11] USSR Contributions to the ITER Specialists Meeting on Operational Limits, June 6-10, 1988

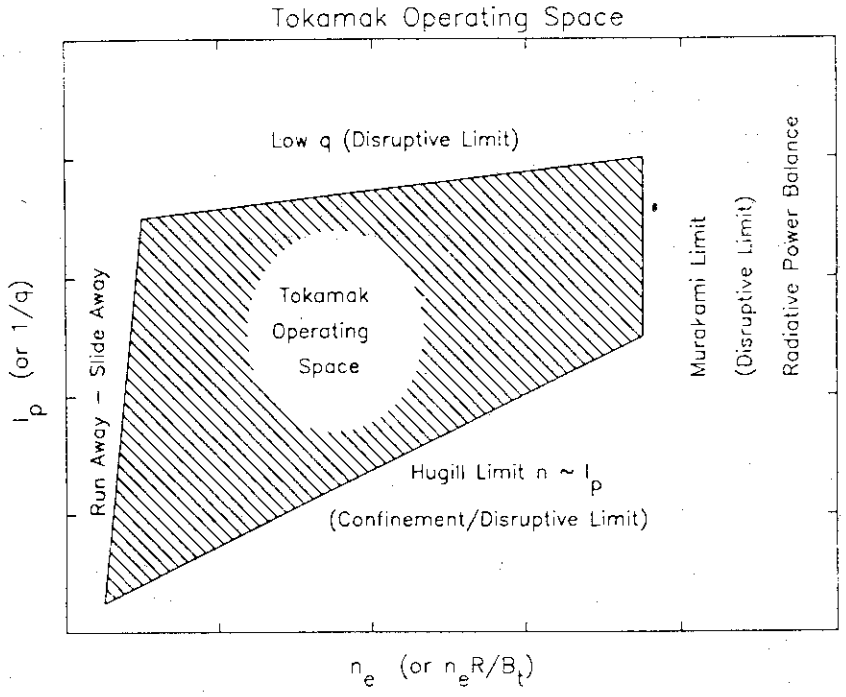

Fig. 1 Schematic view of the tokamak operating space.

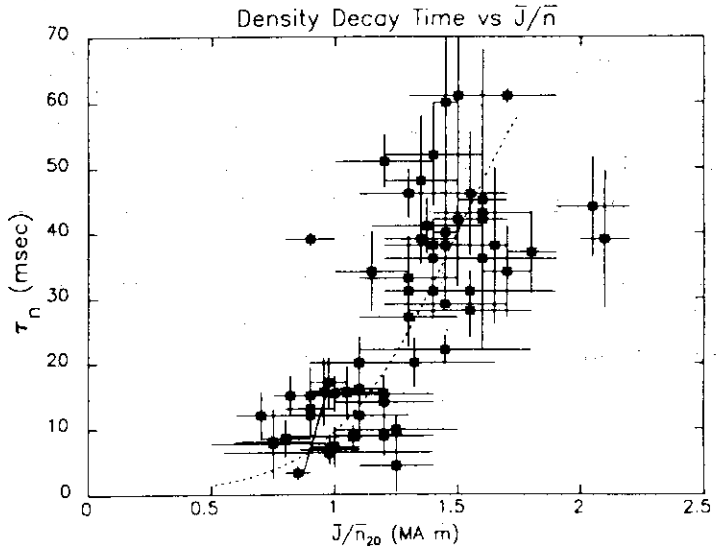

Fig. 2 The density decay time (after pellet injection) versus J/n in Alcator. The density limit is found at (κ=1) J/n=1.

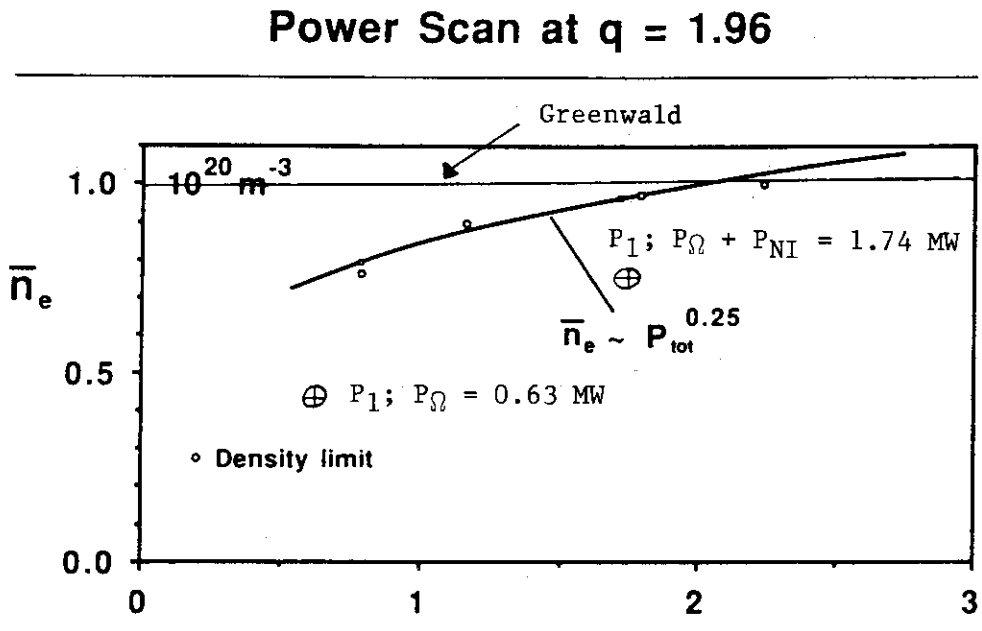

Fig. 3 Critical density versus power at q=2.5 in ASDEX after hardening. The two added points are the ohmic point and the NBI point from a previous study.

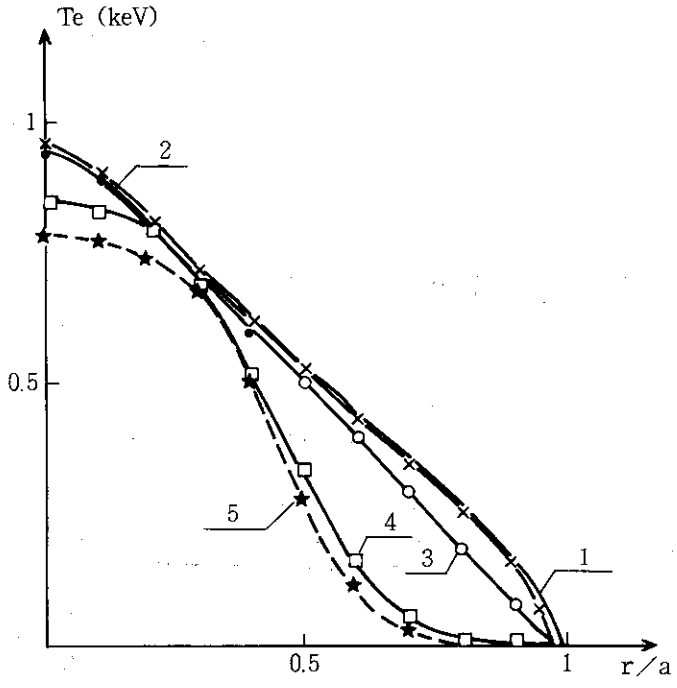

T－10, I_P = 0.25 MA

1 (•) －<ne>= $0.9 \cdot 10^{19}$ m^{-3}

2 (×) －<ne>= $1.5 \cdot 10^{19}$ m^{-3}

3 (○) －<ne>= $2.0 \cdot 10^{19}$ m^{-3}

4 (□) －<ne>= $3.0 \cdot 10^{19}$ m^{-3}

5 (★) －<ne>= $3.3 \cdot 10^{19}$ m^{-3}

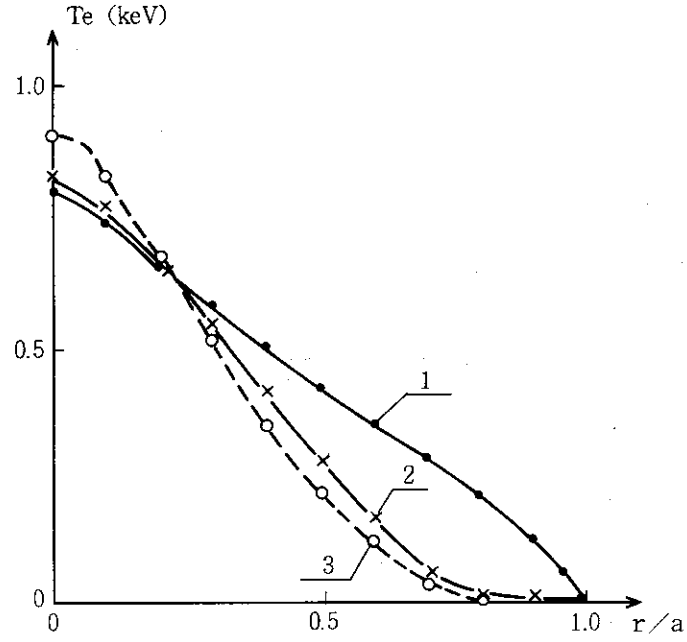

T－10, I_P = 0.45 MA

1 (•) －<ne> $0.9 \cdot 10^{19}$ m^{-3}

2 (×) －<ne> $1.5 \cdot 10^{19}$ m^{-3}

3 (○) －<ne> $2.0 \cdot 10^{19}$ m^{-3}

Fig. 4 Impact of a density increase on the edge temperature in the presence of a transport model according to eq.(8).

Ⅲ. DISRUPTIONS

III.1 Importance for ITER

A major plasma disruption leads to high heat loads on the plasma-facing components and to electro-mechanical shocks on the components and structures surrounding the plasma. Therefore, their presence leads to demanding design requirements for these components and the structures of the device, in particular if a major disruption is a frequent event. Moreover, the present knowledge on disruptions is too limited to characterize, with sufficient accuracy for detailed engineering designs, the heat and force loads and the disruption frequency in ITER.

III.2 Present Knowledge

2.1 Appearance

Major disruptions appear in all tokamaks under various conditions. Particularly relevant for ITER is the experience on large tokamaks and specifically in separatrix-bounded discharges [1 to 12].

A classification of major disruptions can be made according to their cause. They appear
- at the density limit;
- at the q-limit;
- at the β-limit;
- during or just after transient phases, e.g.:
    - fast current ramp-up, often upon growth of locked modes,
    - changes in configuration (such as the transition from a limiter to a separatrix-bounded plasma),
    - large sawtooth crashes, in particular at low q and in the presence of edge localized modes (ELM's),
    - strong ELM activity;
- by "accident", e.g. because of uncontrolled impurity injection into the plasma, hardware failure, human errors in plasma operation, or unknown causes.

The present data base on major disruptions is broadest for disruptions at the density limit.

In present tokamaks, typically 30 % of all discharges end in a hard disruption [5, 9]. A detailed analysis of disruptive shots in JET during the 1986 experimental campaign [9] has shown that in more than half of the disruptive discharges the disruption occurred at reduced current level and therefore did not have important

consequences. About 5 % of all discharges disrupted due to experiments on operational limits (density and q) being conducted and 3 % were caused by mode locking due to inadequate current rampup conditions. Only 6 % of all discharges were disruptive by "accident", that is for reasons which, to some extent, must be considered unavoidable. Also from JT-60 detailed statistical information on the occurrence of disruptions is available [5].

2.2 Evolution of Major Disruptions at the Density Limit in Large Tokamaks

The evolution of a disruption at the density limit in large tokamaks can be subdivided in four phases:

(i)"Pre-precursor": There is a slow evolution of the plasma equilibrium (shrinking of the current channel) induced by the radiative losses approaching or even exceeding the power input, which lasts for typically $\lesssim$ 1 s.

(ii)MHD precursor: Various MHD modes (mostly the m/n = 2/1 mode) grow; in some cases mode locking is observed when the MHD activity has reached a certain level; the duration is typically 100 ms.

(iii)Energy quench ("disruption proper"): After a re-arrangement of the plasma thermal energy over the discharge volume, most of this energy (typically 80%) is lost to the plasma-facing components and the plasma equilibrium adjusts accordingly; the duration of the re-arrangement of the electron thermal energy (in which strong m/n = 1/1 perturbations are seen) is typically a few ms, the deposition time of most of the energy on the plasma-facing components frequently is in the 0.1 ms range (see Figs. 1 and 2a); no direct information on the quench of the ion thermal energy and on the loss of fast ions is available; knowledge on the energy deposition profile is too limited to make a reliable statement; as a consequence of the fast reduction of the plasma pressure, the equilibrium changes: the plasma magnetic axis moves inward and, owing to up/down asymmetries, also fast vertical displacements are observed [3,4]; in DIII - D single-null divertor discharges a typical radial displacement is 3 % of the horizontal minor radius, while the vertical displacement, normally towards the null-point, is typically 15 % of the vertical minor radius (see Fig. 3); a detailed analysis of the reasons for the vertical shift is presently not available.

(iv)Current quench: In the cold impurity-contaminated plasma, that is present after energy quench, first the current tends to increase and a negative voltage spike appears [3, 11], obviously due to a flattening of the current profile which reduces the internal inductance

of the plasma; the duration of this phase is a few ms; thereafter the plasma current decays resistively, accompanied by plasma motion corresponding to an evolving MHD equilibrium (see, e.g. Fig. 3); a detailed analysis of this evolution is not available; in elongated, in particular up-down asymmetic plasmas (e.g. in DIII-D, JET and JT-60) current quench is usually accompanied by appreciable vertical motion [3, 4, 5]; this motion has a time constant similar to that of current quench; in high-q discharges in DIII-D, a vertical displacement by 70 % of the vertical minor radius has been observed with the current decaying only by 30 % [4]; in JT - 60, when the current has decayed by 40 %, the vertical displacement does not exceed more than 30 % of the vertical minor radius [5];there is evidence in DIII-D for the existence of poloidal currents in the vacuum vessel that close through the plasma edge layer during current quench [4]; in vertical disruptions in JET, similar phenomena may have occurred; the energy disipated in the plasma is lost to the first wall, presumably mainly by radiation (see Fig. 2b); eventually the plasma is lost; the rate of current quench can be reduced by efficient plasma position control; there are indications that this rate is enhanced with the plasma current, e.g. in TFTR [7] it increases with I_p^2 while in JT-60 it is linear in I_p [5]; results from JET are given in Fig. 4; it may, however, be that the observed increase of the current quench rate with current is a consequence of limitations in the position control system (see Fig. 4); in JET, typical current quench times lie between a few ms and a few 100 ms, depending on whether or not the plasma develops intense wall contact; during fast current decay in JET, runaway electrons are generated [12] which may carry up to 50% of the original plasma current (the runaway current decays slowly, in 0.1 to 1 s, the runaway electrons being preferentially lost on the inner wall), they contain on the average a fraction $1.8\times10^{-2}\ I_p^{0.6}$(MA) of the poloidal magnetic field energy in the plasma and have energies up to 100 MeV (2% of the poloidal magnetic field energy may be transferred to electrons having energies above 50 MeV);generation of runaway electrons during disruption has also even seen in TFTR [7]; on the other hand, damage of plasma-facing components by runaway electrons was not observable in JT-60 and DIII-D; little is known about the plasma parameters during current quench; in TFTR [7] the electron density first decays with the current, but has a maximum later when the current has decayed to less than half of its initial value.

There is a large scattering in the features of major disruptions, in particular during the phases (iii) and (iv). A strong influence of the plasma configuration is very probable.

Presently, a current quench rate of 1 MA/ms can be considered to be typical for a hard major disruption, but faster decay rates, by a factor cf 10 or more, cannot be excluded. The plasma is anticipated to move inwards and towards the top or bottom of the chamber during current quench.

The provision of efficient position control may be a way to reduce the current quench rate and, consequently, the energy transfer to runaway electrons. It should be investigated whether by providing sufficient space at the inboard side of the plasma, plasma-wall contact can be avoided at the end of energy quench. A double-null divertor configuration appears advantageous in that the radial inward motion of the plasma is not necessarily accompanied by a vertical motion which is anticipated to be uncontrollable; on the other hand, accidental disruptions caused by flakes of divertor target material falling into the plasma may be more frequent in this configuration.

3.3 Disruption Frequency and Disruption Control.

No reliable statement can be made on the frequency of occurrence of major disruptions in ITER. It is obvious though that during the experimental operation in the physics phase of ITER, there will be relatively many more disruptive discharges than during the "routine" operation in the technology phase.

To keep the number of disruptions as low as possible, operation close to operational limits must be avoided. A quantification of this statement will have to be developed. Scenarios for safe startup and shutdown of the discharge will have to be devised accordingly. Disruption control methods (current profile control, feedback control of islands) will have to be developed urgently. Testing their effectiveness in suppressing accidental disruptions is particularly important.

3.4 Source of Information.

The main source of relevant information on disruptions during ITER conceptual design will be JET, PBX-M, DIII-D, JFT-2M, JT-60, and TFTR. Much more specific attention than in the past will have to be paid to disruptions to provide the necessary information.

2.3 Features of Other Disruptions.

While all major disruptions appear to have similar features in phases (iii) and (iv), disruptions other than those at the density limit tend to have quite short MHD precursors (down to a few ms or even less) and pre-precursor phases are absent (or rather are not considered as such: effectively, there is always an evolution of the plasma equilibrium towards unstable conditions preceding a disruption). Specifically low-q disruptions in JET have generally a slower current decay than disruptions at the density limit; the typical duration is a few tens of ms. It is not clear whether this is related to the fact that in low-q discharges the edge electron temperature, before energy quench, is higher or whether the lower internal inductance of these discharges is the distinguishing feature.

III.3 Conclusions and Research Needs

3.1 Energy Quench.

While a range between 0.1 and a few ms for the energy deposition time of the plasma thermal energy on the plasma facing components is an appropriate working hypothesis for ITER, more information is needed before an extrapolation to ITER conditions can be made with confidence. Issues to be elucidated include:

- The mechanism of thermal quench, needed to be able to scale the duration of this phase to ITER and to predict the intensity and the distribution of the heat loads on the plasma-facing components;
- Direct measurements of the heat load distribution on the first wall and limiter/divertor plates for various plasma conditions in present large tokamaks a specifically in separatrix-bounded discharges;
- Direct information on the loss of ion thermal energy and fast ions.

3.2 Current Quench.

Current quench is basically an electrotechnical problem, but the properties of one of the conductors, the plasma, are not well known. To improve the situation, systematic measurements of $T_e(r,t)$ and $Z_{eff}(r,t)$ at the start and during current quench are needed. Also, the energy loss mechanisms (mainly radiation?), the energy deposition profile on the plasma-facing components as well as plasma motion and current flow patterns as a function of time, and runaway electron generation and losses must be elucidated in present large tokamaks before convincing extrapolations to ITER can be done. A full analysis of the experimental material already available now must be performed as soon as possible.

III.4 Specification of Plasma Disruptions

4.1 Plasma Characteristics and Number of Discharges

(i) Physics Phase (ignition studies):

plasma thermal energy	$W_{th,I}$
plasma poloidal magnetic field energy	$W_{m,I}$
energy in fast ions	$W_{f,I} = 0.1\ W_{th,I}$
number of discharges	10^4

(ii) Physics Phase (steady-state operation studies):

plasma thermal energy	$W_{th,ss}$
plasma poloidal magnetic field energy	$W_{m,ss}$
energy in fast ions	$W_{f,ss} = 0.3\ W_{th,ss}$
number of discharges	5.10^3

(iii)Technology Phase (steady-state operation):

plasma thermal energy	$W_{th,TE}$
plasma poloidal magnetic field energy	$W_{m,TE}$
energy in fast ions	$W_{f,TE} = 0.3\ W_{th,TE}$
number of discharges	2.10^4

4.2 Major Disruptions

4.2.1 Number [a], [b] :

4.2.1.1 Physics Phase (ignition studies):

a) thermal and current quench at nominal parameters : 500

b) thermal quench at reduced parameters ($W_{th}^{*}, I = 0.3\ W_{th}, I$), current quench at nominal parameters : 1000

4.2.1.2 Physics Phase (steady-state operation studies) :

thermal and current quench at nominal parameters : 500

4.2.1.3 Technology Phase : 10/300 [c]

[a]) Specifying the number of major disruptions cannot be done just starting from present experience, but must also take into account technical constraints. These show that disruptions, in ITER, must be avoided as far as ever possible. The present working assumption is that during the physics phase only a partially reliable disruption control technique is at hand while in the technology phase a control technique is available which is able to reduce the number of disruptions strongly below the present level.

[b]) The ITER structure should be able to take the mechanical load caused by current quench (see Sect 1.3.2.2.3) for 3.10^4 discharges.

[c]) The two numbers characterize different projections with respect to the reliability of disruption control in the Technology Phase.

4.2.2 Thermal Quench :

Time [ms]	0.1-3 [a]
Total energy:	0.8 W_{th} + W_f ; 0.8 W_{th}^* + W_f in case 4.2.1.1.b
Energy deposition [e]:	
- first wall:	0.4 $W_{th}^{(*)}$ + 1/2 W_f
= the thermal energy (0.4 W_{th}^*) is deposited partly by particles and partly by radiation with a peaking factor:	5
= the fast ion energy (1/2 W_f) is deposited as such with a peaking factor:	5 (or more) [f]
- divertor plates: mainly in the form of particles with an enlarged scrape-off layer width:	0.4 $W_{th}^{(*)}$+1/2 W_f [g] times 3 with respect to normal conditions [g]

[a] The time can vary within this range: design for both extremes.

[e] The distribution of energy deposition is very uncertain.

[f] particularly uncertain (no observations available).

[g] particularly uncertain (data base insufficient) : design for $W_{th}^{(*)}$ + W_f .

4.2.3 Current Quench

Current decay rate [10^9 A/s] [h]: 1 [i]

- Energy deposition [e]:
  - first wall
    - = mainly as radiation: $0.2\ W_{th} + 0.6\ W_m$; $0.2\ W_{th}^* + 0.6\ W_m$ in case 4.2.1.1.b
      - with a peaking factor: 2
    - = as fast (runaway) electrons [j]: $0.1\ W_m$
      - with an energy [MeV]: up to 100
      - and a peaking factor: TBD
  - divertor plates: see footnote [k]
- Plasma horizontal motion:

  for preliminary estimates

  $\Delta R(t) = \Delta R(0) - [a + \Delta R(0)]\ [1 - I_p(t)/I_p(0)]$

  can be used; here $\Delta R(0) = -0.1$ to -0.2m;

  a = horizontal minor radius; I_p = plasma current;

  t = time, with current quench starting at t = 0
- Plasma vertical motion [l]:

  for preliminary estimates

  $\Delta Z(t) = \Delta Z(0) + [b - \Delta Z(0)]\ [1 - I_p(t)/I_p(0)]^{\alpha}$

  can be used; here $\Delta Z(0) = 0$ to 0.6m, $\alpha = 0.5$ to 2;

  q (edge) > 2 must apply; b = vertical minor radius

[h] The plasma current quench is determined by the evolution of the plasma parameters after energy quench, taking account of the electromagnetic coupling to surrounding conducting structures; it depends on the effectiveness of plasma position control. The quench rate given is a typical value, probably at the upper end of the anticipated range, not based on any modelling of the phenomenon. Such a modelling will have to be done, but its reliability will depend on better information to be obtained on the plasma properties at the beginning and during current quench.

4.3 Minor Disruptions

TBD (probably relevant only for steady-state operation $Q \approx 5$)

---

1) With very large scatter: larger values (typically up to 3) must be considered.

3) The fast electron production depends sensitively on the plasma conditions and the current quench rate. Fast electrons are not produced if the current quench rate is kept low. The numbers given are tentative.

4) If the plasma moves vertically the divertor plates may be hit; hence, loads as typical for the first wall should be considered in the design.

5) May be accompanied by anomalous current flow patterns which may allow poloidal currents to flow in the conducting structures surrounding the plasma.

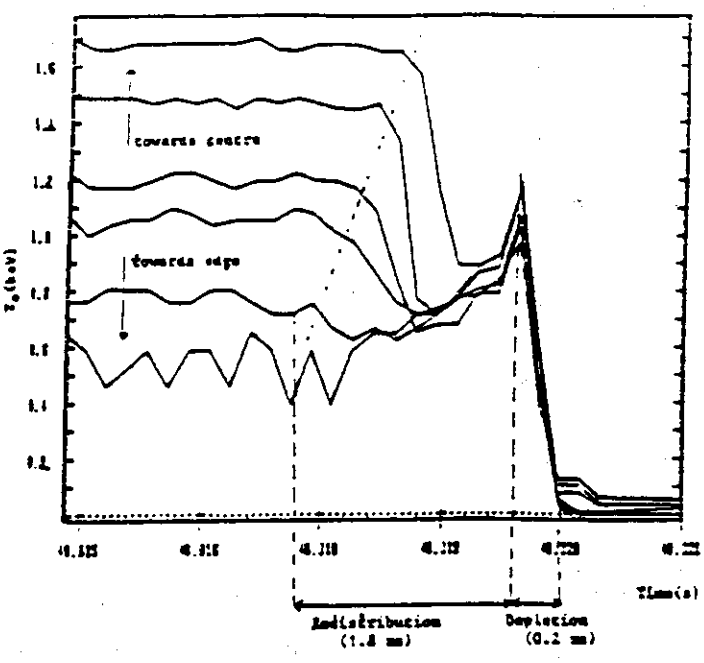

Fig. 1 Time evolution of the electron temperature T_e for various radial positions in JET, deduced from electron cyclotron emission measurements; the time intervals during which the kinetic energy of the plasma is redistributed in radial direction and during which the kinetic energy is lost to the walls are indicated; from Ref.[9].

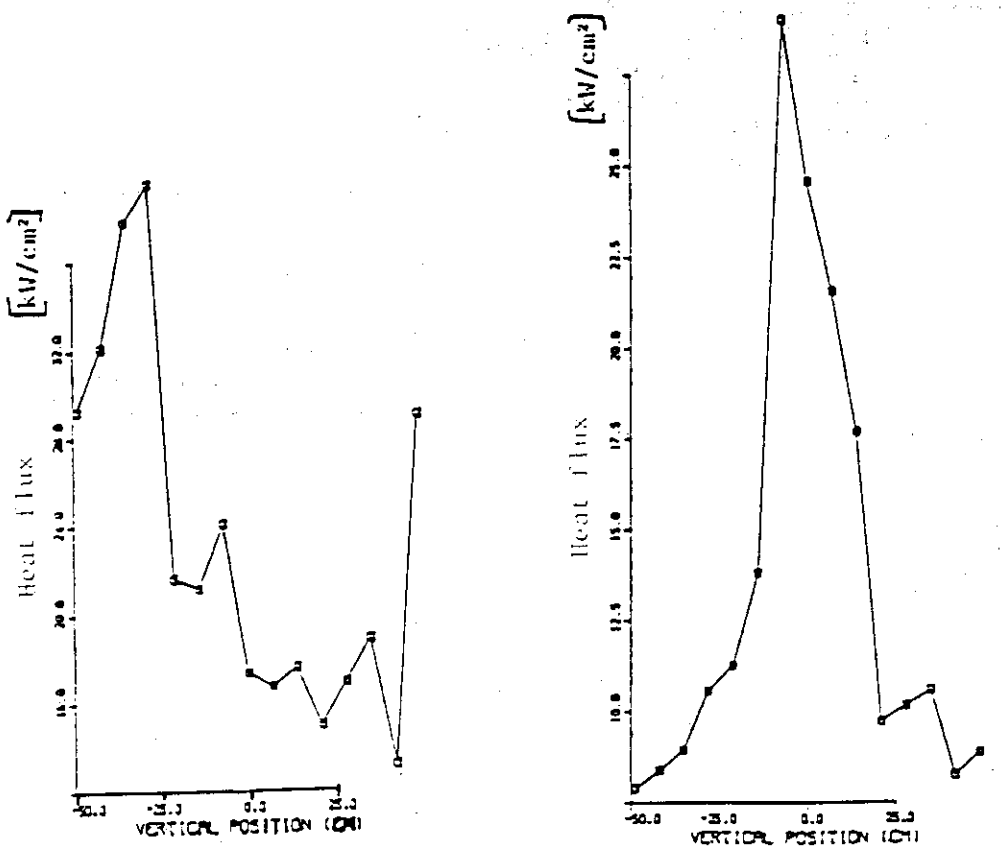

Fig. 2 Heat flux to the inboard wall during a disruption in TFTR as a function of the vertical position [7]:
(a) corresponds to energy quench (t=0.1 ms after the start of the disruption, while (b) is typical for the current quench phase (t=10ms)

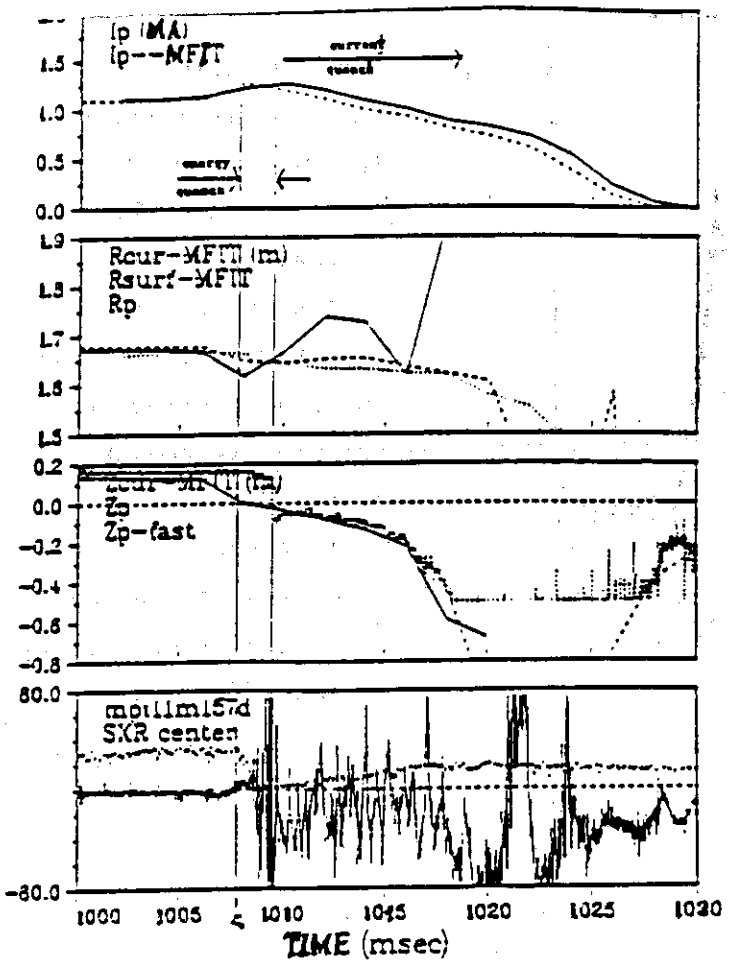

Fig. 3 Horizontal (R_p) and vertical (Z_p) displacement of the plasma magnetic axis in discharge Nr. 55 725 of DIII-D during a disruption initiated at t_o; from Ref. [4].

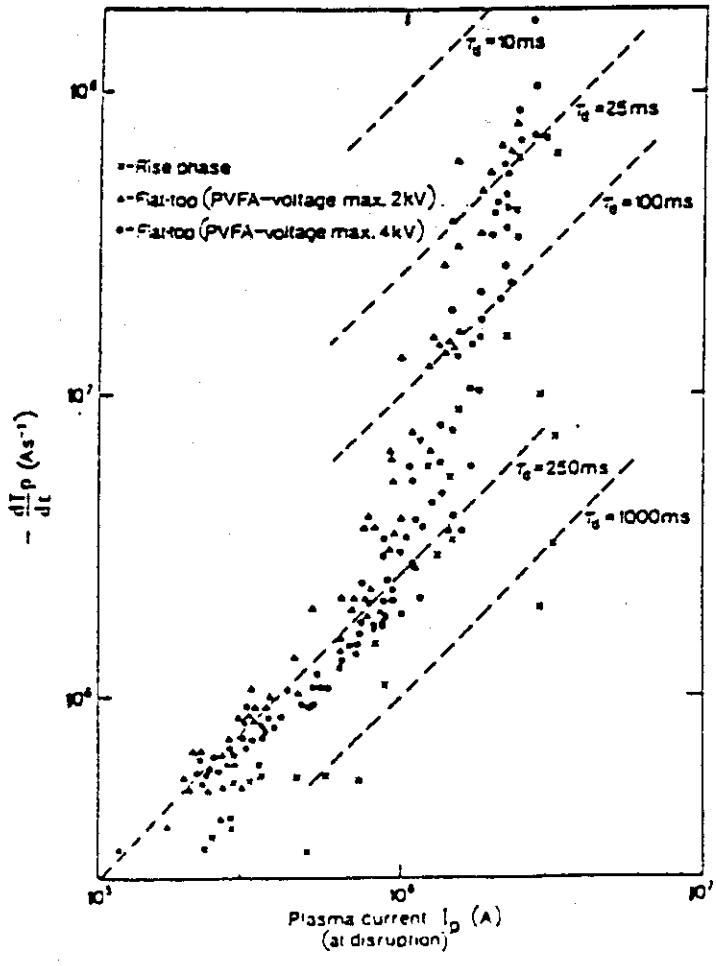

ig. 4 Rate of current decay, $-dI_p/dt$ during a plasma disruption as a function of the plasma current I_p at the moment of disruption: different symbols (x, Δ, ·) are used to distinguish disruptions during current rise and during current flat top for two different values (2 kV and 4 kV) of the maximum voltage of the position control system; τ_d refers to the current decay time; see Ref. [3].

Acknowledgement

The ITER physicists are indebted to many colleagues for their invaluable, direct or indirect contributions to this report. One of the authors, T. Tsunematsu, is grateful to Drs. J. Manickam and L. M. Degtyarev for their suggestions and comments. He is also indebted to Drs. M. Tanaka, S. Tamura, S. Matsuda and T. Takeda for their continuous encouragements during ITER Definition Phase.